CrossMark

Earthquakes in Switzerland and surrounding regions during 2015 and 2016

Tobias Diehl[1] · John Clinton[1] · Nicolas Deichmann[1] · Carlo Cauzzi[1] · Philipp Kästli[1] · Toni Kraft[1] · Irene Molinari[2] · Maren Böse[1] · Clotaire Michel[1] · Manuel Hobiger[1] · Florian Haslinger[1] · Donat Fäh[1] · Stefan Wiemer[1]

Abstract

This report summarizes the seismicity in Switzerland and surrounding regions in the years 2015 and 2016. In 2015, the Swiss Seismological Service detected and located 735 earthquakes in the region under consideration. With a total of 20 earthquakes of magnitude $M_L \geq 2.5$, the seismic activity of potentially felt events in 2015 was close to the average of 23 earthquakes over the previous 40 years. Seismic activity was above average in 2016 with 872 located earthquakes of which 31 events had $M_L \geq 2.5$. The strongest event in the analyzed period was the M_L 4.1 Salgesch earthquake, which occurred northeast of Sierre (VS) in October 2016. The event was felt in large parts of Switzerland and had a maximum intensity of V. Derived focal mechanisms and relative hypocenter relocations of aftershocks image a SSE dipping reverse fault, which likely also hosted an M_L 3.9 earthquake in 2003. Another remarkable earthquake sequence in the Valais occurred close to Sion with four felt events (M_L 2.7–3.2) in 2015/16. We associate this sequence with a system of WNW-ESE striking fault segments north of the Rhône valley. Similarities with a sequence in 2011, which was located about 10 km to the NE, suggest the existence of an en-echelon system of basement faults accommodating dextral slip along the Rhône-Simplon line in this area. Another exceptional earthquake sequence occurred close to Singen (Germany) in November 2016. Relocated hypocenters and focal mechanisms image a SW dipping transtensional fault segment, which is likely associated with a branch of the Hegau-Bodensee Graben. On the western boundary of this graben, micro-earthquakes close to Schlattingen (TG) in 2015/16 are possibly related to a NE dipping branch of the Neuhausen Fault. Other cases of earthquakes felt by the public during 2015/16 include earthquakes in the region of Biel, Vallorcine, Solothurn, and Savognin.

Keywords Seismicity · Magnitude of completeness · Focal mechanisms · Seismotectonics · Rhône-Simplon line · Hegau-Bodensee graben · Basel · Aar massif

Zusammenfassung

Dieser Bericht stellt eine Zusammenfassung der im Jahr 2015 und 2016 in der Schweiz und Umgebung aufgetretenen Erdbeben dar. Im Jahr 2015 wurden vom Schweizerischen Erdbebendienst im erwähnten Untersuchungsgebiet 735 Erdbeben erfasst und lokalisiert. Mit 20 Beben der Magnitude $M_L \geq 2.5$ lag die seismische Aktivität von stärkeren und potentiell spürbaren Ereignissen im Jahr 2015 nahe am Durchschnitt von 23 Beben pro Jahr der vergangenen 40 Jahre. Mit 872 lokalisierten Erdbeben, von denen 31 Ereignisse die Magnitude von M_L 2.5 überstiegen, lag die seismische Aktivität im Jahr 2016 über diesem langjährigen Mittel. Das stärkste Ereignis im untersuchten Zeitraum war das M_L 4.1 Salgesch Beben, welches sich im Oktober 2016 nordöstlich von Sierre (VS) ereignete. Das Beben erreichte eine Intensität V und wurde in grossen Teilen der Schweiz verspürt. Herdmechanismen und Relativlokalisierungen der Nachbeben deuten auf eine nach SSO einfallende Aufschiebung hin, welche

✉ Tobias Diehl
   tobias.diehl@sed.ethz.ch
   http://www.seismo.ethz.ch

1 Swiss Seismological Service, ETH Zürich, Sonneggstrasse 5, 8092 Zurich, Switzerland

2 Department of Earth Sciences, Institute of Geophysics, ETH Zürich, Zurich, Switzerland

Ⓑ Birkhäuser

vermutlich auch mit einem M_L 3.9 Beben im Jahr 2003 zusammenhängt. Mit vier verspürten Ereignissen (M_L 2.7–3.2) ereignete sich nahe Sion eine weitere bemerkenswerte Sequenz von Erdbeben im Wallis. Diese Sequenz steht in Verbindung mit einem WNW-OSO streichenden Verwerfungssystem nördlich des Rhonetals. Ähnlichkeiten mit einer Sequenz die sich im Jahr 2011 etwa 10 km nordöstlich ereignete, deuten auf eine en-échelon Anordnung von Verwerfungen im kristallinen Grundgebirge hin, die in diesem Bereich dextrale Verschiebungen entlang der Rhone-Simplon-Linie aufnimmt. Eine weitere außergewöhnliche Sequenz von Erdbeben wurde im November 2016 nahe Singen (Deutschland) aufgezeichnet. Relokalisierte Hypozentren und Herdmechanismen deuten auf eine in südwestliche Richtung einfallende transtensive Verwerfung hin, welche vermutlich ein Bruchsegment des Hegau-Bodensee Grabens darstellt. Mikroseismizität am westlichen Rand dieses Grabens im Jahr 2015/16 steht möglicherweise in Verbindung mit einem nach Nordosten einfallenden Segment der Neuhausen-Verwerfung nahe Schlattingen (TG). Weitere Erdbeben, die von der Bevölkerung zwischen 2015 und 2016 verspürt wurden, waren unter anderem Beben in den Regionen Biel, Vallorcine, Solothurn und Savognin.

Résumé

Ce rapport résume l'activité sismique en Suisse et dans les régions limitrophes au cours des années 2015–2016. En 2015, le Service Sismologique Suisse a détecté et localisé 735 séismes dans la zone considérée. Avec un total de 20 séismes de magnitude $M_L \geq 2.5$, l'activité sismique potentiellement ressentie a été proche de la moyenne de 23 événements sur les 40 années précédents. L'activité sismique a été supérieure à la moyenne en 2016 avec 872 séismes localisés, dont 31 événements avec $M_L \geq 2.5$. L'événement le plus fort de la période analysée a été le séisme de Salquenen (M_L 4.1) qui s'est produit au nord-est de Sierre (VS) en octobre 2016. Cet événement a été ressenti dans une grande partie de la Suisse avec une intensité maximale de V. Les mécanismes au foyer obtenus et la relocalisation relative des hypocentres des répliques permettent de visualiser une faille inverse à pendage S.-S.-E. qui a probablement également généré un séisme de magnitude M_L 3.9 en 2003. Une autre séquence remarquable en Valais s'est produite près de Sion avec quatre événements ressentis (M_L 2.7-3.2) en 2015–2016. Nous associons cette séquence à un système de segments de failles orientés O.-N.-O./E.-S.-E. au nord de la vallée du Rhône. Des similitudes avec la séquence de 2011, localisée à environ 10 km au N.-E., suggèrent l'existence d'un système de failles en échelon dans le socle qui accommode le déplacement dextre le long de la faille du Simplon dans cette zone. Une autre séquence exceptionnelle s'est produite près de Singen (Allemagne) en novembre 2016. La relocalisation des hypocentres et les mécanismes au foyer permettent de visualiser un segment de faille transtensive avec un pendage vers le S.-W. qui est probablement associé à une branche du graben de l'Hegau-Bodensee. A l'extrémité ouest de ce graben, des microséismes près de Schlattingen (TG) en 2015/16 sont possiblement reliés à une branche à pendage N.-E de la faille de Neuhausen. D'autres tremblements de terre ont été ressentis par la population en 2015/16 dans les régions de Bienne, Vallorcine (France), Soleure et Savognin.

1 Introduction

Past earthquake activity in Switzerland and surrounding regions has been documented in a series of annual reports since 1879. A detailed overview on the history of past reports and studies covering different aspects of the recent seismicity of Switzerland is given e.g. by Diehl et al. (2014). The present report first summarizes the state of the seismic network and documents changes in its configuration during 2015 and 2016. Then we give a short overview on the methods used for earthquake analysis. This is followed by a description of the seismic activity and significant earthquakes in 2015/16. The discussion of significant earthquakes and earthquake sequences considers information from derived focal mechanisms and high-precision relative hypocenter relocations.

2 Data acquisition and analysis

2.1 Seismic stations in operation during 2015/16

The Swiss Seismological Service at ETH Zurich (SED) operates two separate nationwide seismic networks, a high-gain seismometer network predominantly consisting of broad-band instruments (SDSNet, Table S-1 in the Electronic Supplement) and a low-gain accelerometer network (SSMNet, Table S-2 in the Electronic Supplement) (Swiss Seismological Service (SED) at ETH Zurich 1983). A more complete description can be found in previous Annual Reports (e.g., Diehl et al. 2014). In addition, the SED operates a number of temporary stations for various projects (Table S-3 in the Electronic Supplement). SED operated permanent stations with on-line data acquisition that were operational at the end of 2016 are shown in Fig. 1.
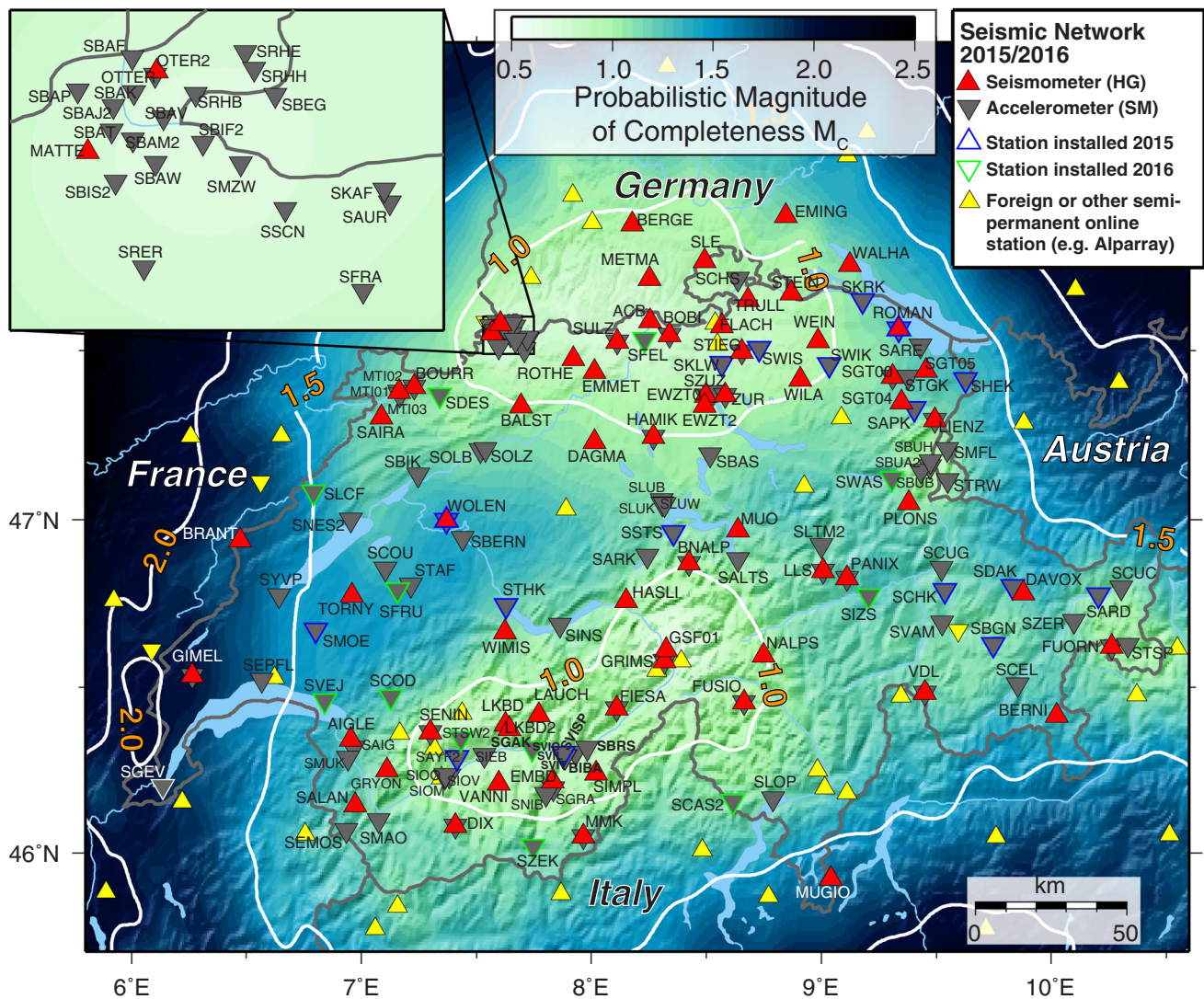
Fig. 1 Seismograph stations in Switzerland and surrounding regions with on-line data acquisition operational at the end of 2016. Stations of the "Switzerland Seismological Network" (network code "CH") are indicated with labels. The stations defined as high-gain (HG) are mostly equipped with broad-band or 5-s sensors, whereas the strong-motion stations (SM) are accelerometers (see also Table S-1–S-3 in the Electronic Supplement). Yellow triangles mark complementary permanent or temporary stations with real-time data acquisition, used to improve detection and location of seismicity. Colors projected onto the topographic relief in the background show the lateral variation of the magnitude of completeness (M_C) for on-line stations operating at the end of 2016, assuming a detection probability of 0.99, a minimum number of 6 automatic triggers, and a hypothetical focal depth of 5 km. Bold, white lines indicate M_C contours of 1.0, 1.5 and 2.0

Within the Swiss Strong Motion Network (SSMNet) renewal project, 100 free-field, real-time, very broad-band accelerometer stations are being installed over a 10-year timeframe between 2010 and 2019 (Clinton et al. 2011; Michel et al. 2014). In 2015/16, 26 new strong motion stations were installed (Fig. 1; 14 in 2015: SAPK, SARD, SAYF2, SBGN, SCHK, SDAK, SHEK, SKLW, SKRK, SMOE, SSTS, STHK, SWIK, SWIS; 12 in 2016: SCAS2, SCOD, SDES, SFEL, SFRU, SGAK, SIZS, SLCF, STSW2, SVEJ, SWAS, SZEK). In 2015, SVISP (located in the town of Visp (VS), see Fig. 1) was built as part of the

COGEAR project (Fäh et al. 2012). SVISP is a borehole array with three triaxial-borehole accelerometers at different depths down to 102 m below the surface, a free-field surface accelerometer, and a string of 6 pore water pressure sensors operating down to a depth of 21 m.

The broadband network is also undergoing a renewal period that continued during 2015 and 2016. Numerous stations were upgraded by replacement of the acquisition hardware and broadband sensor, and if not already existing, the addition of a strong motion sensor. In 2015, two additional borehole stations were installed in NW

Switzerland (Fig. 1). Both stations ROMAN (99 m depth) and WOLEN (134 m depth) are equipped with broadband borehole sensors at depth and a strong motion sensor at the surface. The short period borehole sensor EWZT0, installed at the Triemli-Spital in Zurich in November 2009 at 250 m depth for monitoring the deep geothermal project of Elektrizitätswerke Zürich (EWZ), was reactivated and integrated into the SDSNet. A surface strong motion sensor was added at this site. The networks built to monitor potential sites for radioactive waste disposal; the geothermal projects in Basel (2006) and Sankt Gallen (2013); and the Mont Terri and Grimsel Rock Laboratories continue to operate.

In 2015/16, temporary stations from the AlpArray Seismic Network (AASN) (Molinari et al. 2016; AlpArray Seismic Network 2015) were deployed in the greater Alpine region. AlpArray is a large-scale scientific project to improve our understanding of the orogenesis and seismic hazard in the wider Alpine Region (http://www.alparray. ethz.ch). The targeted station spacing of 40 km for broadband seismometers means that around 250 temporary stations will complement the over 400 existing permanent stations operated by seismic networks in the greater Alpine region. In Switzerland three stations were added to achieve the required density (A060A, A061A, and A062A). The number of AlpArray stations operating outside but near the Swiss border in Italy, France, Austria and Germany is significant, and these stations are included in the national monitoring when possible.

To improve the reliability of locations for events at the periphery of or outside of Switzerland, the SED continues to be engaged in an on-going cross-frontier cooperative effort to exchange seismic data in real-time with foreign seismic networks as documented in detail by Diehl et al. (2014). Over 60 foreign stations were monitored by the SED at the end of 2016, boosted by the addition of new permanent stations in France and the aforementioned AlpArray stations.

2.2 Automatic earthquake detection and magnitude of completeness during 2015/16

All stations with real-time data acquisition (Fig. 1) were used for automatic real-time detection of seismic events. An estimation of the magnitude of completeness (M_C) achieved by the network configuration at the end of 2016 is shown in Fig. 1. The M_C magnitude is defined as the lowest magnitude of events that a network is able to record reliably and completely (e.g., Schorlemmer and Woessner 2008). We use the probabilistic approach of Schorlemmer and Woessner (2008) to compute lateral variations in M_C (see Electronic Supplement for details).

The map shown in Fig. 1 assumes a probability of detection of 0.99, a hypothetical focal depth of 5 km and a minimum number of 6 automatic triggers, which corresponds to the minimum number currently required by the monitoring system of the SED (Diehl et al. 2013). Compared to previous M_C maps of Switzerland (e.g., Nanjo et al. 2010; Kraft et al. 2013), the recent and ongoing densification of the seismic network has significantly improved the detection capabilities throughout Switzerland. The completeness magnitude achieved by the network configuration at the end of 2016 is $M_C = 1.5$ for most parts of Switzerland and $M_C = 1.0$ in north and southwest Switzerland (Fig. 1). Regions of relatively higher M_C are the western Molasse basin and the southwestern Jura Mountains with M_C between 1.5 and 2.0.

2.3 Routine and supplementary earthquake analysis

Methods and software currently used for routine earthquake analysis are described in detail in Diehl et al. (2013, 2014). In 2015, the software used to generate broadband moment tensor inversions was migrated to a SeisComP3 module 'scmtv', as described in Vackář et al. (2017). For selected sequences in 2015/16, a cross-correlation based template matching method was performed in order to lower the detection threshold of micro-seismicity. The applied procedure is described in Diehl et al. (2015). To resolve active fault planes and to image the spatio-temporal evolution for selected earthquake sequences, we performed relative hypocenter relocations using the double-difference method of Waldhauser and Ellsworth (2000) in combination with waveform cross-correlation. The applied procedure is described in Diehl et al. (2017).

3 Seismic activity during 2015 and 2016

3.1 Overview

During 2015, the SED detected and located a total of 735 earthquakes in the region shown in Fig. 2a. Based on criteria such as the time of occurrence, the location, and signal character or on direct communication, 125 additional seismic events were identified as quarry blasts. Magnitude values of the earthquakes recorded in 2015 range from $M_L - 0.1$ to 3.3 (Fig. 3). During 2016, 872 earthquakes and 189 quarry blasts were detected and located by the SED in the same region (Fig. 2b, 3). The magnitudes of earthquakes in 2016 range from $M_L - 0.6$ to 4.1 (Fig. 3). The events with $M_L \geq 2.5$ in 2015/16 are listed in Table 1. The chosen magnitude threshold of M_L

2.5 ensures that the data set is comparable to seismicity in the same magnitude range for previous years (completeness magnitude $M_C = 2.5$ for Switzerland over the period 1975–2016; Nanjo et al. 2010), and makes sure that the number of unidentified quarry blasts and of mislocated earthquakes is negligible.

Tables 1 and 2 list location qualities for events with $M_L \geq 2.5$, the criteria used to assign the quality rating for the given locations, as well as the corresponding estimated location uncertainties. Location quality criteria defined in Table 2 provide first-order information on the reliability of epicenter location and focal depth and allow the comparison with locations documented in previous annual reports. For events, which occurred after 2013, additional nonlinear location uncertainty estimates are provided in the digital version of the catalog (quakeML format, https://quake.ethz.ch/quakeml), available online (www.seismo.ethz.ch). The reported uncertainties, however, do not account for systematic errors, e.g. errors in the seismic velocity model used for location, or, misidentified phases (e.g., Husen and Hardebeck 2010). Ignoring the contribution of such errors can result in a significant underestimation of the true location accuracy. On the other hand, these errors are usually difficult to assess (e.g., Husen and Hardebeck 2010). Therefore we provide conservative uncertainty estimates on hypocenter accuracy in the discussion of significant earthquakes. These estimates consider the nonlinear uncertainty estimates as well as tests with varying subsets of data (P and/or S phases, different distance ranges, with/without refracted Pn phases, etc.) and velocity models.

Fault-plane solutions based on first-motion polarities of events in 2015/16 are shown in Figs. 4, 5, and 6 (see also Fig. 2), and their parameters are listed in Table S-4 in the Electronic Supplement. Only well-constrained solutions are listed and first-order uncertainties of the first-motion mechanisms are provided by the spread of solutions in Figs. 4–6. Following the definition of Aki and Richards (2002), the parameters strike, dip and rake are used to define fault-orientations in this report. The strike angle is measured clockwise from north, with the fault dipping down to the right of the strike direction. The dip angle is measured down from the horizontal. The slip direction is defined by the rake angle, measured in the fault plane as the angle between the directions of strike and slip. Three events in 2016 generated sufficient long-period energy to produce a high-quality full-waveform moment-tensor inversion (Fig. 6). Moment magnitudes derived from this procedure range between M_W 3.2 and M_W 3.7. Additional M_w values derived from the spectral fitting method of Edwards et al. (2010) are listed in Table 1.

Figure 7 shows the epicenters of the 984 earthquakes with $M_L \geq 2.5$, which have been recorded in Switzerland and surrounding regions over the period 1975–2016. These events represent about 6% of the total number of events detected during that time in the same area. The majority of earthquakes with $M_L \geq 2.5$ in 2015/16 occurred in regions, which have been seismically active in previous years (Fig. 7). In the following section we discuss significant and noteworthy earthquakes and earthquake sequences during the period 2015/16.

3.2 Significant earthquakes of 2015 and 2016

3.2.1 Gelterkinden (BL), 2015

On January 17th 2015, an M_L 2.8 earthquake occurred close to the town of Gelterkinden (BL) (Fig. 2a). This earthquake was part of a sequence, which was active since at least June 2014. In total, 20 additional events with magnitudes ranging from M_L 0.3 to M_L 1.8 are located in a radius of 2 km around the M_L 2.8 event in the period between 2000 and 2015. The seismicity is located at a depth of about 10 km and therefore clearly within the crystalline basement. The mechanism shown in Fig. 4a suggests a NW–SE striking normal fault, similar to other mechanisms in this region (Zeglingen und Läufelfingen, see e.g., Deichmann et al. 2000). The sequence was characterized by remarkably similar waveforms, which allowed relative hypocenter relocation using high-resolution differential times calculated from waveform cross-correlation. Cross-sections through the relocated seismicity (Fig. S-1 in the Electronic Supplement) suggest that the plane steeply dipping towards the NE was the active plane.

3.2.2 Biel/Bienne (BE), 2015

More than 300 felt reports were received for the M_L 3.1 earthquake, which occurred about 7 km west of Biel/Bienne (BE) on January 31st 2015 (Fig. 2a). The M_L 3.1 earthquake was followed by a series of events in the first half of 2015. The largest of these events had a magnitude of M_L 2.7 (Table 1). These earthquakes were part of a cluster of earthquakes already active in January 2014 (Diehl et al. 2015). Focal depths in both sequences are in the range of 8–10 km. The focal mechanism associated with the event in January 2015 indicates normal faulting with the T-axis oriented NE-SW (Fig. 4c, Table S-4), similar to the two mechanisms derived for the sequence in 2014 (Diehl et al. 2015). In summary, the Biel/Bienne sequence of 2014/15 documents NE-SW directed extension in the crystalline basement beneath the southern edge of the Jura.

3.2.3 Basadingen-Schlattingen (TG), 2015

On May 31st 2015, an earthquake of M_L 2.2 occurred close to the town of Basadingen-Schlattingen (TG)

(Figs. 2a, 8a). This event is the largest amongst a small cluster of 11 earthquakes, which occurred between 2014 and 2016 at this location. The focal depths of these events range from 5 to 7 km. A precursory S-to-P converted phase is visible in the recordings of the closest station TRULL, which is located 4.6 km from the epicenter (Fig. S-2 in the Electronic Supplement). This precursory phase suggests that the earthquake occurred below the sedimentary cover, which is about 1–2 km thick in this region (e.g., Nagra 2008). The focal mechanism derived from first motion polarities of P-waves is consistent with a NW–SE striking normal fault (Fig. 4f). The "upward" polarity at the closest station TRULL, however, does not fit this mechanism (Fig. 4f). The take-off angles for this mechanism are calculated in the regional 3D velocity model of Husen et al. (2003). An unresolved velocity contrast (e.g. basement-sediment transition) or unresolved basement topography (e.g. Permo-Carboniferous trough structures) below the station TRULL could lead to an overestimation of the take-off angle. A potentially smaller take-off angle would move the observation at TRULL towards the compressional quadrant of the focal sphere and might therefore explain the apparent misfit.

To resolve the active fault plane associated with this sequence, additional events were detected by applying the template-matching algorithm of Hermann et al. (2017) to continuous waveform data of station TRULL. This procedure was already applied to several sequences in the year 2014 and is described in Diehl et al. (2015). As a result, additional 12 events could be located. In total, 21 events could be used for double-difference relocation, and the resulting relative relocations are shown in Figs. 8b, c. The relative relocations in combination with the focal mechanism suggest a NE dipping normal fault (dip of about 40°, see Fig. 4f) in the crystalline basement (depth of about 5–6 km). The two events in 2014 appear disconnected from the cluster of events in 2015/16 but it cannot be excluded that they occurred on the same NE-dipping structure. Assuming a constant dip of the fault, the expected surface outcrop would locate several kilometers SW of the epicenters (Fig. 8a). Considering a possible uncertainty in the absolute locations of earthquakes in the order of several hundred meters, it is possible that the structure imaged by micro-earthquakes is related to the Neuhausen fault, which is mapped as a NE-dipping extensional feature in the Mesozoic sediments and forms the westernmost bounding fault of the Hegau-Bodensee Graben (Fig. 8a) (e.g., Egli et al. 2016; Madritsch 2015). The depth of the micro-earthquakes suggests a continuation of this structure into the crystalline basement.

Fig. 2 Epicenters and focal mechanisms of earthquakes recorded by ▶ the Swiss Seismological Service: **a** during 2015; **b** during 2016. Events and focal mechanisms (lower hemisphere projections) discussed in the text (bold labels) are Basadingen-Schlattingen (BAS), Bernina Pass (BER), Biel (BIE), Crans (CRA), Diemtigen (DIE), Gelterkinden (GLK), Göschenen (GOE), Hilzingen (HIL), Jungfrau (JFR), Mulegns (MUL), Novel (NOV), Salgesch (SAL), Solothurn (SOL), St-Léonard (STL), Vallorcine (VAL). Additional events with focal mechanisms are Guarda (GRD), Lenzkirch (LEK), Klösterle a. Arlberg (KAA), Rebévelier (REB), Schluderns (SLU), Schopfheim (SHO), Stein am Rhein (SAR). Background colors outline major tectonic units: Molasse basin of the northern Alpine foreland (yellow ocher), Jura Mountains (turquois), Alps (gray), external massifs (light red), southern Rhine graben (brown). Gray lines indicate faults and fault systems adopted from Heuberger et al. (2016), Mock and Herwegh (2017), Vouillamoz et al. (2017), and Swisstopo (2005). *AM* Aar massif, *EF* Engadine fault, *FF* Fribourg fault zone, *PF* Pontarlier fault zone, *RSL* Rhône-Simplon line, *SgF* St. Gallen fault zone, *SoF* Solothurn fault zone. Boxes outline Hegau-Bodensee and Rhône Valley regions discussed in text

3.2.4 The earthquake sequence of St. Léonard (VS), 2014-2016

Between 2014 and 2016, a remarkable sequence of more than 120 locatable earthquakes occurred in the Valais close to Sion, about 2 km northeast of the village St. Léonard (Figs. 2a, b, 9a). The sequence initiated in January 2014 and several episodes of enhanced seismic activity occurred since then. The four strongest events (M_L 2.7–3.2, Table 1) were felt by local residents. About 280 felt reports were received for the strongest earthquake of the sequence (M_L 3.2), which occurred on June 24th 2016. Focal depths within the sequence range between 6 and 9 km, indicating that the seismicity is most likely located in the crystalline basement below the southern edge of the Helvetic nappes. Focal mechanisms derived for the four strongest events are dominantly strike slip (Figs. 4g, 5f, g, l, 9b).

Relative relocations shown in Fig. 9b image a linear, WNW-ESE striking seismogenic structure of about 0.6 km length. Its general strike is consistent with the strike of the dextral planes of the May 2016 and the June 2016 mechanisms (Fig. 9b). Seismicity initiates at the ESE edge of the structure, and events in 2014 cluster around the future M_L 3.1 earthquake of June 2015. Following the M_L 3.1 earthquake of 2015, seismicity migrates towards WNW, culminating in the M_L 2.9 and M_L 3.2 events in May and June 2016. The M_L 2.7 earthquake of November 2016 appears to be "out-of-sequence", filling the gap between the events of May and June 2016 (Fig. 9b). The mechanism of the November 2016 event results in a larger reverse component since the strike of the dextral plane is rotated counterclockwise with respect to the other mechanisms (Fig. 9b). The spatio-temporal character of the sequence, as well as the potential variations in the focal mechanisms, suggest the existence of a dextral fault system consisting of several
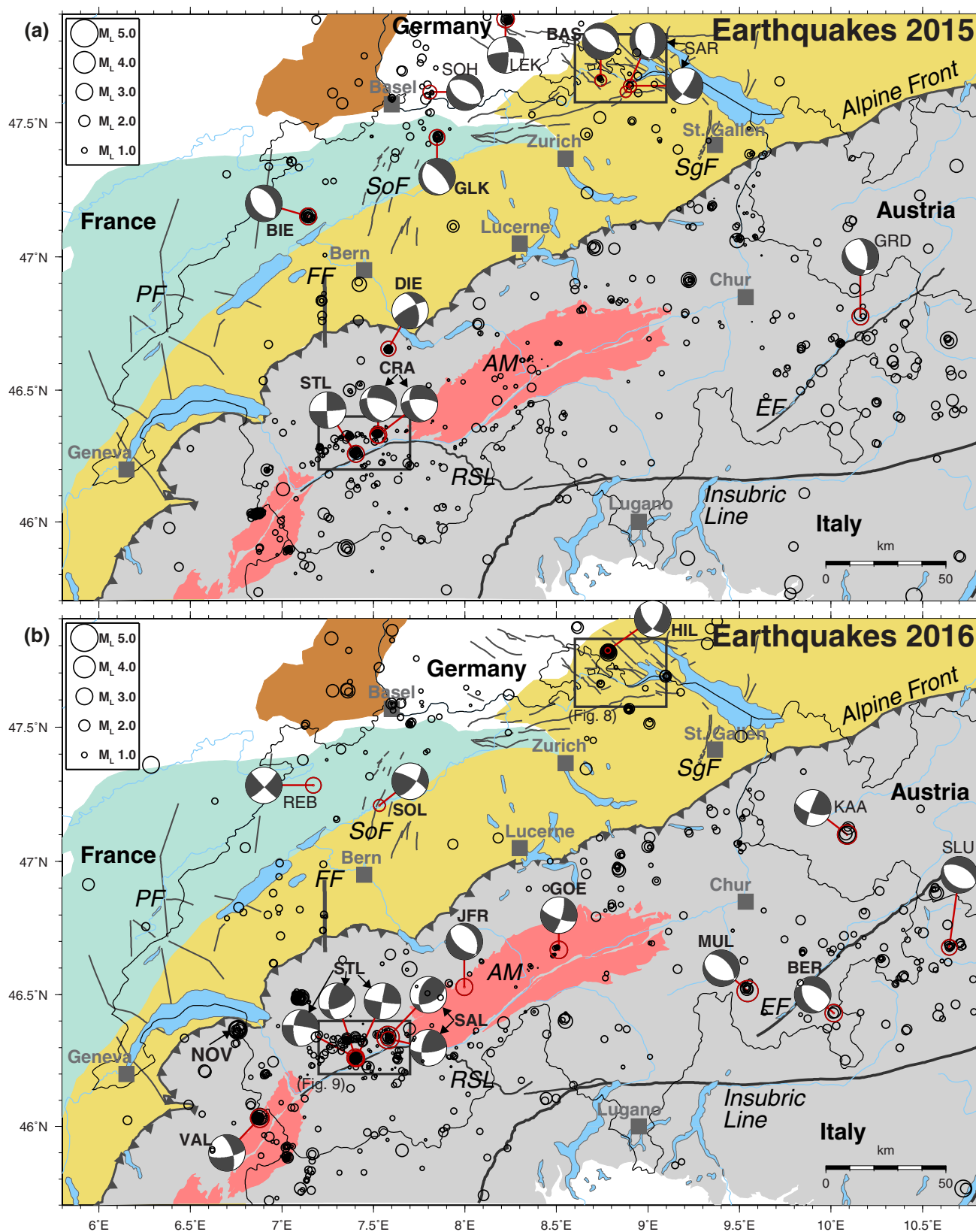
Fig. 3 Earthquake activity during 2015 (blue) and 2016 (red): **a** timeline showing magnitude of each event, cumulative number of events, and average number of events per year (563 events) in the period 2002–2014 (horizontal dashed gray line); **b** magnitude histogram
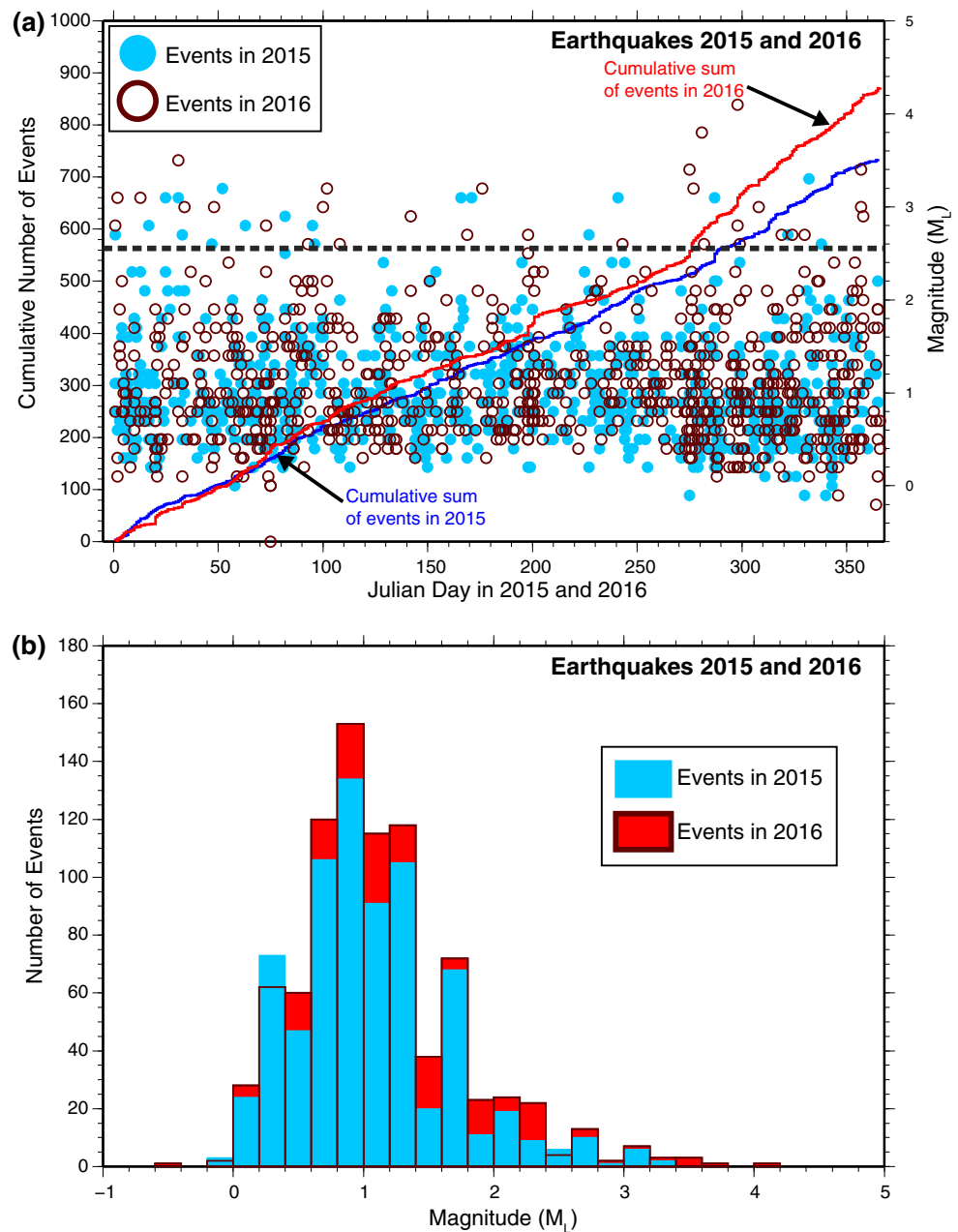
segments or branches rather than one single fault. A skew in strike combined with the enlarged reverse component of the November 2016 mechanism might indicate a step-over structure between two segments or a small-scale restraining bend along a longer segment. On a larger scale, position, orientation and kinematics of the St. Léonard structure resemble the Sierre sequence of 2011, which was located about 10 km further to the NE (Deichmann et al. 2012). This similarity suggests the existence of an en-echelon WNW-ESE oriented Riedel fault type system of basement faults below the northern edge of the Rhône valley, compatible with WSW-ENE oriented dextral slip along the Rhône-Simplon line in this area (Fig. 9a). Additional

evidence for such en-echelon systems is provided by geologically mapped similarly oriented surface structures shown in Fig. 9a (Cardello and Mancktelow 2015).

3.2.5 Diemtigen (BE), 2015

The M_L 2.7 earthquake of August 15th 2015 is part of the Diemtigen sequence, which initiated in 2014 (Diehl et al. 2015) (Fig. 2a). Its focal depth of 10 km and the derived oblique focal mechanism (strike-slip with reverse component; Fig. 4i, Table S-4) are evidently similar to oblique solutions derived for events in 2014 (Diehl et al. 2015). Based on this similarity, we conclude that the active plane

Table 1 Earthquakes with $M_L \geq 2.5$ during 2015 and 2016

Date and time (UTC)	Lat. (°N)	Lon. (°E)	X/Y (km)	Z (km)	Mag. (M_L)	Mag. (M_{WSPEC})	Q	Location
2015/01/01 09:44:27	46.915	9.222	736/197	4	2.7	2.7	B	Piz Segnas, GL
2015/01/17 09:16:53	47.446	7.848	631/255	10	2.8	2.4	A	Gelterkinden, BL (**GLK**)
2015/01/25 17:34:27	46.777	10.160	808/184	7	3.1	3.1	A	Guarda, GR (**GRD**)
2015/01/31 21:54:02	47.152	7.143	578/222	10	3.1	2.9	A	Biel/Bienne, BE (**BIE**)
2015/02/02 04:05:18	47.155	7.143	578/223	10	2.7	2.6	A	Biel/Bienne, BE
2015/02/16 14:06:10	45.862	9.216	738/080	6	2.6	2.7	B	Erba, I
2015/02/21 22:23:58	47.883	8.222		24	3.2	2.7	A	Lenzkirch, D (**LEK**)
2015/03/04 06:13:15	47.035	8.711	697/210	0	2.8	2.9	B	Mythen, SZ
2015/03/23 03:58:11	45.718	10.453	835/067	10	2.9	2.9	A	Lago d'Idro, I
2015/03/23 13:27:15	47.428	6.133	501/254	16	2.5	2.4	A	Schopfheim, D (**SOH**)
2015/04/05 14:20:55	46.618	10.527	836/167	16	2.8	2.7	C	Rioz, F
2015/04/06 13:18:51	46.898	7.422	599/194	6	2.6	2.7	A	Köniz, BE
2015/06/15 03:14:47	45.901	7.351	593/083	2	3.1	3.0	B	Mont Gelé, I/VS
2015/06/20 10:30:23	46.260	7.404	597/123	9	3.1	2.9	A	St-Léonard, VS (**STL**)
2015/08/15 18:34:16	46.656	7.581	611/167	10	2.7	2.6	A	Diemtigen, BE (**DIE**)
2015/08/29 13:07:19	46.689	10.643	845/176	9	3.1	3.1	A	Schluderns, I
2015/10/14 00:13:45	46.331	7.525	607/131	4	3.1	3.1	A	Crans, VS (**CRA**)
2015/11/18 08:10:41	46.328	7.522	606/131	5	2.7	2.8	A	Crans, VS (**CRA**)
2015/11/28 21:29:57	45.762	9.797	783/070	12	3.3	3.2	A	Albino, I
2015/12/04 03:12:40	47.062	9.487	756/214	6	2.6	2.6	A	Balzers, FL
2016/01/01 12:22:41	47.285	7.171	580/237	18	2.8	2.6	A	Rebévelier, BE (**REB**)
2016/01/02 10:42:45	46.529	7.997	643/153	7	3.1	2.9	A	Jungfrau, BE/VS (**JFR**)
2016/01/13 02:13:37	47.361	6.284	513/246	17	3.1	2.9	C	Baume-les-Dames, F
2016/01/31 22:43:59	47.101	10.087	801/220	6	3.5	3.4	B	Klösterle a. Arlberg, A (**KAA**)
2016/02/03 21:37:39	45.764	10.723		9	3.0	2.9	B	Lago di Garda, I
2016/02/17 20:17:04	47.101	10.087	801/220	5	3.0	2.9	B	Klösterle a. Arlberg, A
2016/03/13 00:58:49	46.679	10.646	845/175	9	2.8	2.8	A	Schluderns, I (**SLU**)
2016/04/02 16:47:41	46.882	10.575	839/197	6	2.6	2.6	B	Nauders, A
2016/04/09 21:19:43	46.038	6.879	557/098	5	3.0	2.9	A	Vallorcine, F
2016/04/11 10:47:23	46.431	10.015	798/145	8	3.2	3.1	A	Bernina Pass, GR (**BER**)
2016/04/17 23:40:59	46.035	6.875	556/098	5	2.6	2.7	A	Vallorcine, F
2016/05/21 03:49:38	46.258	7.407	597/123	8	2.9	2.8	A	St-Léonard, VS (**STL**)
2016/06/17 12:06:46	46.597	7.697	620/161	7	2.7	2.7	A	Frutigen, BE
2016/06/24 04:12:17	46.262	7.402	597/123	8	3.2	3.1	A	St-Léonard, VS (**STL**)
2016/07/16 02:36:39	46.490	7.108	575/149	5	2.7	2.9	A	Château-d'Oex, VD
2016/07/16 04:54:53	46.486	7.108	575/148	4	2.5	2.6	A	Château-d'Oex, VD
2016/08/30 05:37:05	47.635	7.359	594/276	11	2.6	2.7	A	Mulhouse, F
2016/10/01 23:17:39	46.033	6.879	557/098	5	3.4	3.3	A	Vallorcine, F (**VAL**)
2016/10/03 06:43:43	46.669	8.513	682/169	5	3.2	3.1	B	Göschenen, UR (**GOE**)
2016/10/07 07:27:07	46.514	9.544	761/153	10	3.8	–	A	Mulegns, GR (**MUL**)
2016/10/08 02:31:60	46.400	8.549	685/139	4	2.6	–	B	Val Bavona, TI
2016/10/24 14:44:12	46.338	7.580	611/132	8	4.1	3.7	A	Salgesch, VS (**SAL**)
2016/10/24 14:45:04	46.343	7.580	611/132	8	2.8	–	A	Salgesch, VS
2016/10/25 01:42:14	46.334	7.580	611/131	8	2.6	2.5	A	Salgesch, VS (**SAL**)
2016/11/03 05:48:22	47.775	8.784	701/292	7	3.0	2.9	B	Hilzingen, D (**HIL**)
2016/11/14 02:06:45	47.779	8.783	701/293	7	2.7	2.6	B	Hilzingen, D
2016/11/19 00:53:56	47.780	8.782	701/293	5	2.7	2.6	A	Hilzingen, D (**HIL**)
2016/11/25 18:29:02	46.260	7.403	597/123	8	2.7	2.5	A	St-Léonard, VS (**STL**)

Table 1 (continued)

Date and time (UTC)	Lat. (°N)	Lon. (°E)	X/Y (km)	Z (km)	Mag. (M_L)	Mag. (M_{WSPEC})	Q	Location
2016/12/22 19:24:15	46.367	6.757	547/135	− 1	3.0	2.8	B	Novel, F **(NOV)**
2016/12/22 19:50:17	46.368	6.759	548/135	0	3.4	3.4	B	Novel, F **(NOV)**
2016/12/23 09:54:23	46.369	6.759	548/135	− 2	2.9	2.9	B	Novel, F **(NOV)**

The values listed under M_{WSPEC} are the moment magnitudes calculated from the spectral fitting method documented in Edwards et al. (2010). The quality rating (Q) is defined in Table 2. Bold three-letter abbreviations in the last column correspond to labels used for focal mechanisms in Figs. 2, 4, 5, 6, and Table S-4

Table 2 Criteria and location uncertainty corresponding to the quality rating (Q) of the hypocentral parameters in the event list in Table 1

Rating (Q)	Criteria		Uncertainty	
	GAP (degrees)	DM (km)	H (km)	Z (km)
A	≤ 180	≤1.5 × Z	≤ 2	≤ 3
B	≤ 200	≤ 25	≤ 5	≤ 10
C	≤ 270	≤ 60	≤ 10	> 10
D	> 270	> 60	> 10	> 10

GAP largest angle between epicentre and two adjacent stations, *DM* minimum epicentral distance, *H* horizontal location, *Z* focal depth

of the 2015 event is the ENE dipping plane (Fig. 4i), which was imaged already by the 2014 sequence (Diehl et al. 2015). In 2015, additional 30 earthquakes of the Diemtigen sequence were detected and located. The main activity occurred between July and September 2015. In 2016, only one event was located.

3.2.6 Crans (VS), 2015

On October 14th 2015, an M_L 3.1 earthquake occurred in the region of Crans-Montana (VS), about 4 km north of Sierre (Figs. 2a, 9a). With a depth of 4–5 km, the event is likely located in the uppermost part of the crystalline basement. However, with the given uncertainties in focal depth (in the order of ± 1–2 km) a source in the lower part of the sedimentary cover (e.g. within the autochthonous Mesozoic sediments) cannot be entirely excluded. On November 18th 2015, an M_L 2.7 earthquake occurred in the vicinity of the October event. The focal mechanisms derived for both events are of transtensional character and virtually identical (Figs. 4j, l, 9c, Table S-4). Relative relocations of all events located during 2015 around the two events suggest that the WNW-ESE striking plane was the active one (Fig. 9c). The WNW-ESE strike of the seismogenic structure agrees well with the overall strike of the St. Léonard sequence (Fig. 9b) and correlates in orientation and kinematics with a set of WNW striking faults mapped by Cardello and Mancktelow (2015) in the Helvetic nappes (set (2) in Fig. 9a). This correlation suggests a
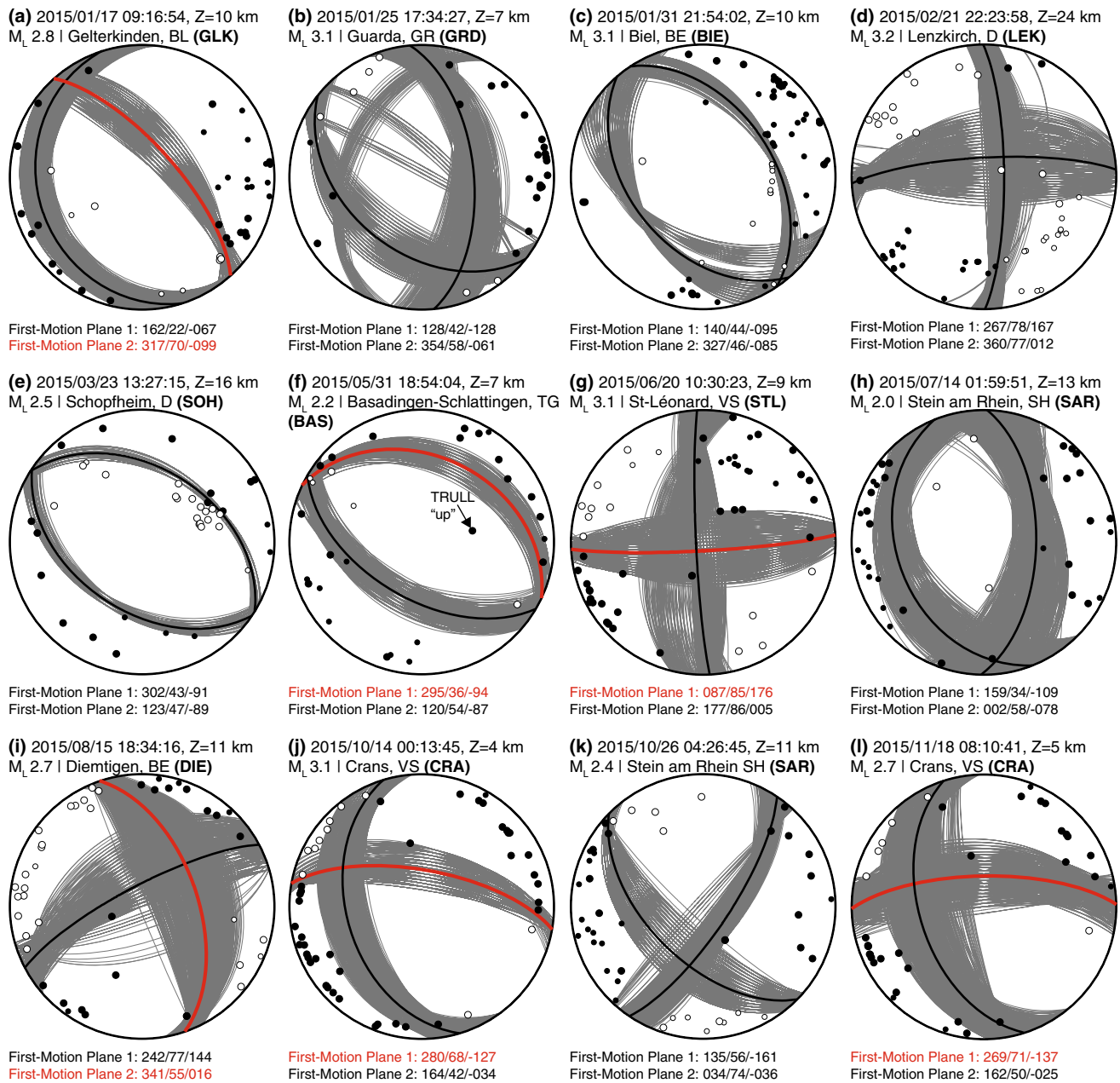
possible connection of seismogenic faults in the basement with outcropping faults observed at the surface of the Helvetic nappes.

3.2.7 Jungfrau (BE/VS), 2016

The epicenter of the January 2016 M_L 3.1 earthquake was located about 3 km ESE of the Jungfrau summit (Fig. 2b) in the border region of canton Bern and Valais. The focal depth of 7 km indicates a source within the Aar massif. Since reliable fault plane solutions are sparse within the massif, the derived focal mechanism (Fig. 5b, Table S-4) provides important information on the internal neotectonic deformation of the Aar massif. The normal fault mechanism suggests NE-SW oriented extension in its northern part, which is oriented approximately parallel to the general strike of the Aar massif (Fig. 2b). The orientation of P and T-axes is comparable to the mechanism of the Lötschental earthquake of 1997, which suggests similarly directed extension within the Aar massif (Deichmann et al. 1998). As described by Deichmann et al. (1998), however, the fault plane solution of the 1997 Lötschental earthquake was largely constrained by relative P- and S-wave amplitudes of the seismograms and first-motion polarities alone would also allow for a pure strike-slip mechanism. Therefore the orientation of the P-axis is less certain for the 1997 Lötschental event, and the few available mechanisms do currently not allow conclusions on whether neotectonic deformation within the Aar massif is dominated by strike-slip or normal faulting.

3.2.8 Bernina Pass (GR), 2016

The M_L 3.2 earthquake of April 2016 was located about 2 km NNE of the Bernina Pass (Fig. 2b). Its focal depth is relatively well constrained by P- and S-phases observed at station BERNI, which is located within 2 km distance of the epicenter. The derived fault plane solution corresponds to an almost pure normal faulting mechanism (Fig. 5e, Table S-4), and the NE-SW orientation of the T-axis is consistent with other normal fault mechanisms, which have been observed in the Austroalpine domain since 1988 (e.g.,

(a) 2015/01/17 09:16:54, Z=10 km
M_L 2.8 | Gelterkinden, BL **(GLK)**

First-Motion Plane 1: 162/22/-067
First-Motion Plane 2: 317/70/-099

(b) 2015/01/25 17:34:27, Z=7 km
M_L 3.1 | Guarda, GR **(GRD)**

First-Motion Plane 1: 128/42/-128
First-Motion Plane 2: 354/58/-061

(c) 2015/01/31 21:54:02, Z=10 km
M_L 3.1 | Biel, BE **(BIE)**

First-Motion Plane 1: 140/44/-095
First-Motion Plane 2: 327/46/-085

(d) 2015/02/21 22:23:58, Z=24 km
M_L 3.2 | Lenzkirch, D **(LEK)**

First-Motion Plane 1: 267/78/167
First-Motion Plane 2: 360/77/012

(e) 2015/03/23 13:27:15, Z=16 km
M_L 2.5 | Schopfheim, D **(SOH)**

First-Motion Plane 1: 302/43/-91
First-Motion Plane 2: 123/47/-89

(f) 2015/05/31 18:54:04, Z=7 km
M_L 2.2 | Basadingen-Schlattingen, TG **(BAS)**

TRULL "up"

First-Motion Plane 1: 295/36/-94
First-Motion Plane 2: 120/54/-87

(g) 2015/06/20 10:30:23, Z=9 km
M_L 3.1 | St-Léonard, VS **(STL)**

First-Motion Plane 1: 087/85/176
First-Motion Plane 2: 177/86/005

(h) 2015/07/14 01:59:51, Z=13 km
M_L 2.0 | Stein am Rhein, SH **(SAR)**

First-Motion Plane 1: 159/34/-109
First-Motion Plane 2: 002/58/-078

(i) 2015/08/15 18:34:16, Z=11 km
M_L 2.7 | Diemtigen, BE **(DIE)**

First-Motion Plane 1: 242/77/144
First-Motion Plane 2: 341/55/016

(j) 2015/10/14 00:13:45, Z=4 km
M_L 3.1 | Crans, VS **(CRA)**

First-Motion Plane 1: 280/68/-127
First-Motion Plane 2: 164/42/-034

(k) 2015/10/26 04:26:45, Z=11 km
M_L 2.4 | Stein am Rhein SH **(SAR)**

First-Motion Plane 1: 135/56/-161
First-Motion Plane 2: 034/74/-036

(l) 2015/11/18 08:10:41, Z=5 km
M_L 2.7 | Crans, VS **(CRA)**

First-Motion Plane 1: 269/71/-137
First-Motion Plane 2: 162/50/-025

Fig. 4 Fault-plane solutions based on first-motion polarities for 12 earthquakes in 2015 (see Table S-4 in the Electronic Supplement). All stereograms are lower hemisphere, equal-area projections. Solid circles correspond to compressive first motion (up); empty circles correspond to dilatational first motion (down). The take-off angles were computed with the NonLinLoc software (Lomax et al. 2000), using the 3D velocity model of Husen et al. (2003). Gray lines show sets of acceptable solutions derived by the HASH algorithm (Hardebeck and Shearer 2002); black bold lines indicate the (preferred) average focal mechanisms of all accepted solutions; red bold lines mark the active plane as determined from high-precision relative earthquake relocations. Information on origin time (UTC time), focal depth in km below mean sea level (Z), region (same label as in Fig. 2 and Table S-4) and the two focal planes (defined by strike, dip, rake) is provided above and below each mechanism. See text for definition of strike, dip and rake

Marschall et al. 2013). Only the upward polarity observed at station BERNI appears inconsistent with the derived solution (Fig. 5e). This misfit is likely due to an error in the computed take-off angle, which at close epicentral distances is very sensitive to even small errors in location, focal depth and the velocity model.

3.2.9 Solothurn (SO), 2016

On August 20th 2016, an M_L 2.2 earthquake occurred below the city center of Solothurn (Fig. 2b). Despite its low magnitude it was felt by local residents and more than 100 felt reports were received for this event. The relatively
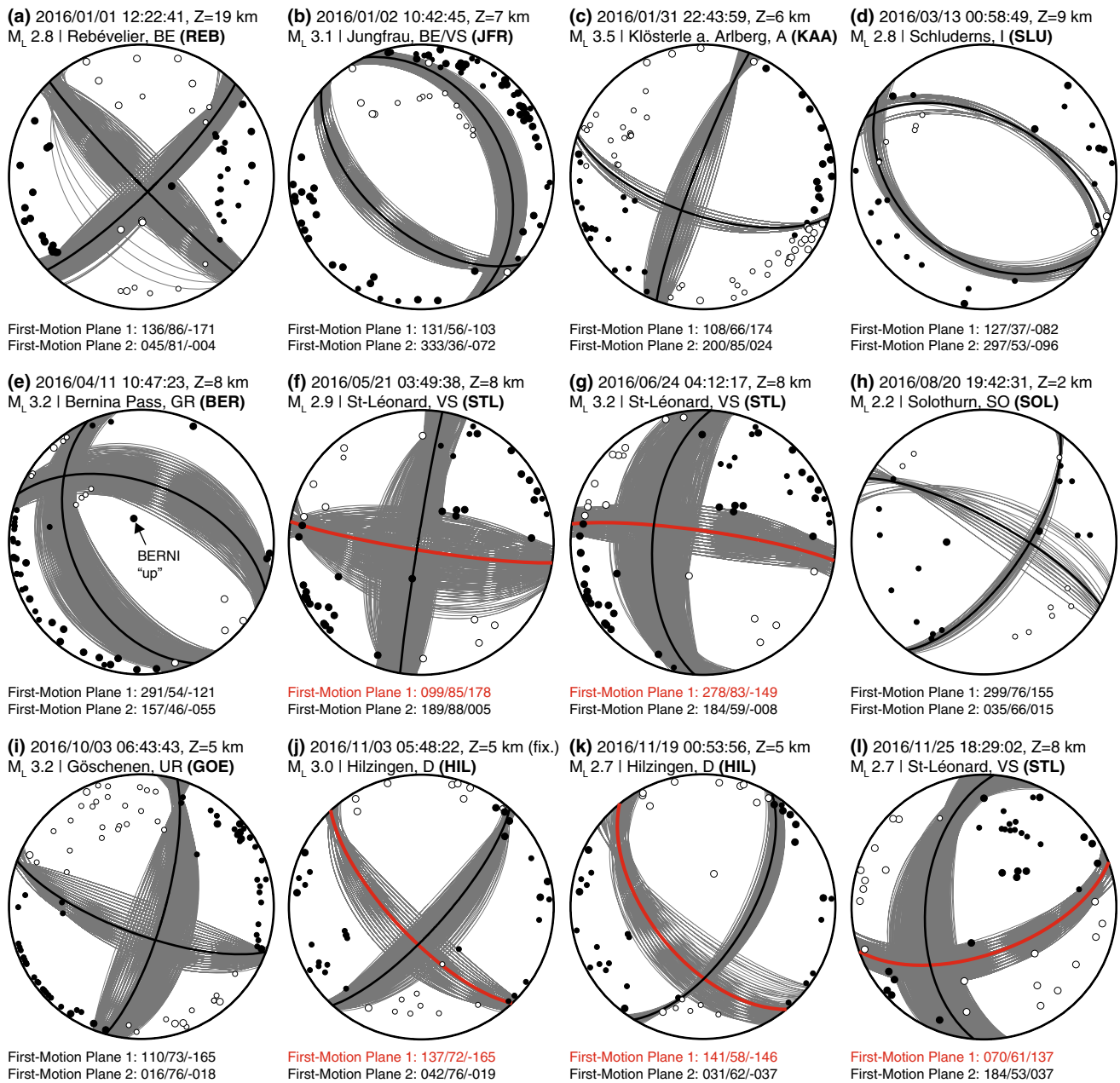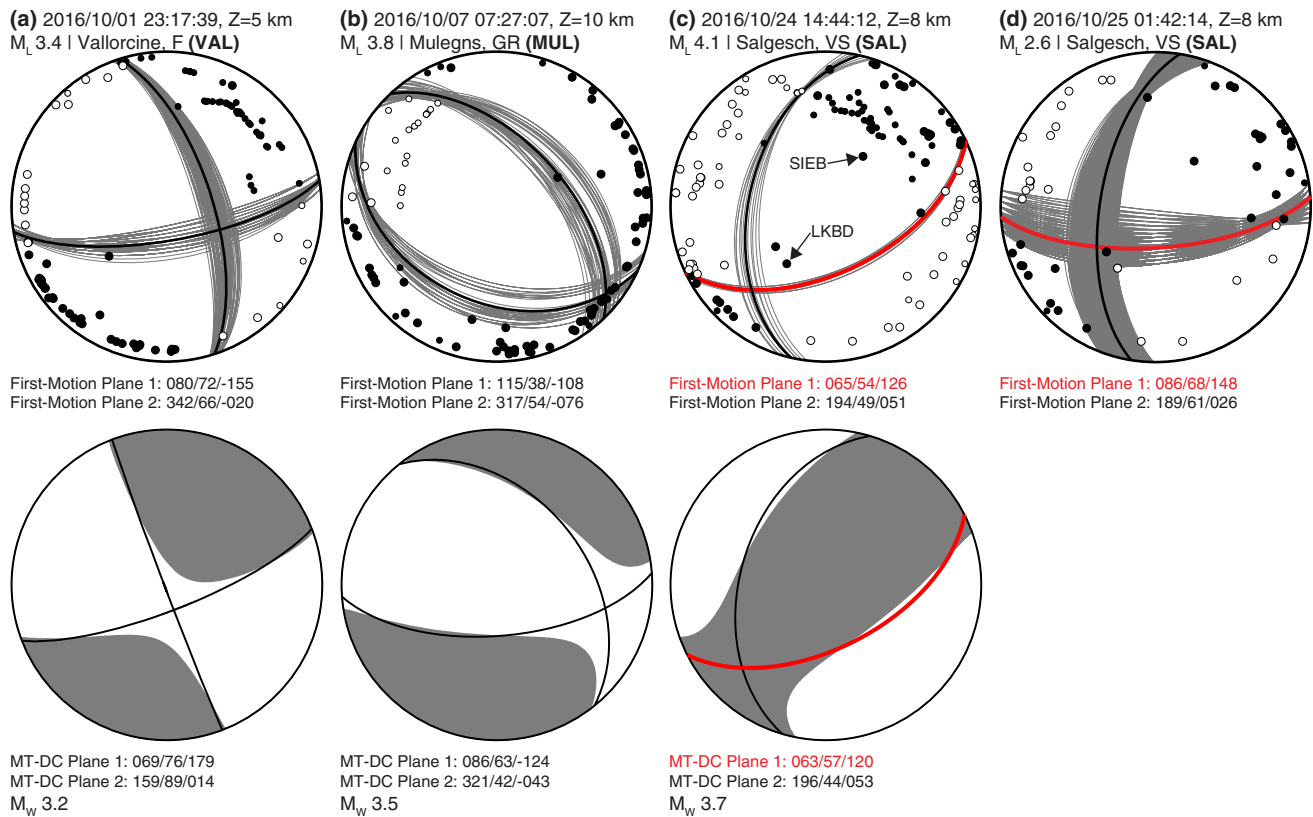
Fig. 5 Fault-plane solutions (lower hemisphere projections) based on first-motion polarities for 12 earthquakes in 2016 (see Table S-4). Symbols and explanation as in Fig. 4

high intensity of this event suggests a very shallow source. With the two strong-motion stations SOLZ and SOLB located within 1 km distance from the epicenter, the calculated focal depth of 2 km is well constrained. The top of the crystalline basement is at about 2 km depth in this area and it is likely that the event is located within the sedimentary cover (Mock and Herwegh 2017). The Solothurn Fault Zone (SoF, Fig. 2b) is mapped as a NNE-SSW striking left-lateral fault zone in the Mesozoic sediments (Mock and Herwegh 2017). The left-lateral strike-slip fault plane solution of the M_L 2.2 earthquake (Fig. 5h,

Table S-4) agrees well with the orientation and kinematics of the SoF. Therefore we associate this event with the main strand or a branch of the SoF.

3.2.10 Vallorcine (France), 2016

The M_L 3.0 earthquake of April and the M_L 3.4 earthquake of October 2016 (Fig. 2b) are part of the on-going earthquake sequence that followed the M_L 4.9 earthquake of September 2005 (e.g., Deichmann et al. 2006; Fréchet et al. 2010; Diehl et al. 2013, 2015; Cara et al. 2017). Both these

(a) 2016/10/01 23:17:39, Z=5 km
M_L 3.4 | Vallorcine, F **(VAL)**

First-Motion Plane 1: 080/72/-155
First-Motion Plane 2: 342/66/-020

(b) 2016/10/07 07:27:07, Z=10 km
M_L 3.8 | Mulegns, GR **(MUL)**

First-Motion Plane 1: 115/38/-108
First-Motion Plane 2: 317/54/-076

(c) 2016/10/24 14:44:12, Z=8 km
M_L 4.1 | Salgesch, VS **(SAL)**

SIEB
LKBD

First-Motion Plane 1: 065/54/126
First-Motion Plane 2: 194/49/051

(d) 2016/10/25 01:42:14, Z=8 km
M_L 2.6 | Salgesch, VS **(SAL)**

First-Motion Plane 1: 086/68/148
First-Motion Plane 2: 189/61/026

MT-DC Plane 1: 069/76/179
MT-DC Plane 2: 159/89/014
M_W 3.2

MT-DC Plane 1: 086/63/-124
MT-DC Plane 2: 321/42/-043
M_W 3.5

MT-DC Plane 1: 063/57/120
MT-DC Plane 2: 196/44/053
M_W 3.7

Fig. 6 Lower hemisphere projections of first-motion fault-plane solutions (top row) and corresponding full-waveform moment tensor (MT) solutions (bottom row) for 4 earthquakes in 2016 (see Table S-4). Symbols and explanation of first-motion mechanism as in Fig. 4. Black bold lines on the moment tensor indicate the double-couple part of the MT solution. Red bold lines on the MT solution mark the active plane as determined from high-precision relative earthquake relocations. Strike/Dip/Rake of the double-couple part of the MT (MT-DC) as well as the associated moment magnitude (M_W) are provided below the MT solution. No MT solution is available for the M_L = 2.6 Salgesch aftershock (d)

2016 events were felt by the local population. Focal depths and the strike-slip fault plane solutions (Fig. 6a) are very similar to the ones of past events of this sequence. For the M_L 3.4 event, we were able to calculate a moment tensor solution (Fig. 6a) with a moment magnitude of M_W 3.2.

3.2.11 Göschenen (UR), 2016

The M_L 3.2 earthquake, which occurred on October 3rd 2016, is located about 5 km west of the village of Göschenen (Fig. 2b). Besides the Jungfrau event, this is the second significant earthquake located within the Aar massif in 2016. Compared to the normal fault mechanism of the Jungfrau earthquake (Fig. 5b), the fault plane solution of the Göschenen event indicates an almost pure strike-slip mechanism (Fig. 5i, Table S-4). The NE-SW orientation of the T-axis is consistent with the solution derived for the Jungfrau event and therefore suggests along-strike extension within the Aar massif. The WNW-ESE orientation of the dextral plane of the focal mechanism (strike 110°, Fig. 5i) correlates with the strike of dextral shear zones

mapped in the central Aar massif, which are associated with the Oberaar deformation phase (e.g., Wehrens et al. 2017). This correlation suggests a possible reactivation of pre-existing shear zones within the present-day stress field in the Aar massif.

3.2.12 Mulegns (GR), 2016

With a magnitude of M_L 3.8, the second largest earthquake in the period 2015/16 occurred on October 7th 2016, west of the Surses valley in the southern part of the canton Graubünden (Fig. 2b). The epicenter was located about 5 km west of the village of Mulegns and the earthquake was felt in a radius of about 100 km (Fig. 10a). The SED routinely runs the USGS ShakeMap software (Worden et al. 2010; Worden and Wald 2016) to automatically compute maps of ground shaking for every earthquake with $M_L \geq 2.5$ within the greater Swiss region. The ShakeMap is computed as described in Cauzzi et al. (2015), using the Swiss ground-motion model of Edwards and Fäh (2013), combined with regional site amplification factors (Fäh
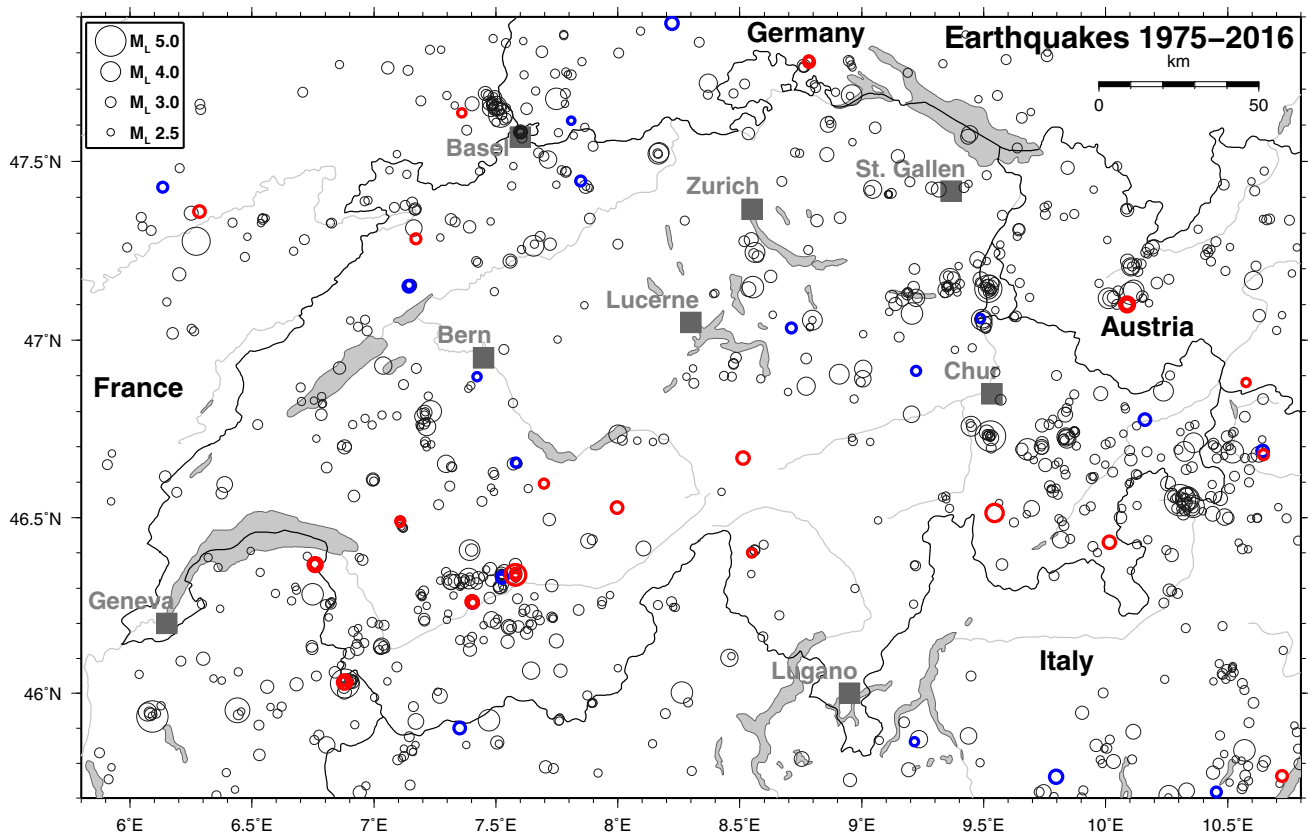
Fig. 7 Epicenters of earthquakes with magnitudes $M_L \geq 2.5$, during the period 1975–2016. Gray circles denote earthquakes in the period 1975–2014; bold blue circles indicate earthquakes in 2015; red circles indicate earthquakes in 2016

et al. 2011) and station recordings. Macroseismic intensity is converted from measured peak ground velocity using the equations of Faenza and Michelini (2010). The maps in Fig. 10 show the spatial distribution of the interpolated macroseismic intensity along with observed macroseismic intensities based on felt reports from online questionnaires. The final macroseismic field depicted in the ShakeMap of Fig. 10 results from a weighted average of the predicted ground-motions, the station recordings and the felt reports. Colors in Fig. 10a are proportional to macroseismic intensity levels according to the European Macroseismic Scale (EMS-98; Grünthal 1998) and indicate that the M_L 3.8 earthquake of October 7th reached an intensity of IV.

The mainshock was preceded by an M_L 1.8 earthquake on October 5th, and only six aftershocks with magnitudes between M_L 0.9 and M_L 2.3 were detected by routine procedures. The region was seismically active prior to the M_L 3.8 event with about 30 events since 1984 within a radius of 6 km. The station closest to the mainshock was VDL (Fig. 1) at a distance of only 8 km. The focal depths of mainshock and aftershocks were therefore well constrained and range between 9 and 11 km. This depth range indicates a source in the upper basement of the Penninic domain (e.g., Marschall et al. 2013). The fault plane

solution derived for the mainshock is close to a pure normal fault mechanism (Fig. 6b, Table S-4). The corresponding moment tensor solution differs slightly from the first-motion solution (Fig. 6b). The main difference is the larger strike-slip component in the moment tensor solution. On the other hand, strike and dip of the NE dipping plane (plane #2 in Fig. 6b) agree remarkably well between the two solutions. The moment magnitude derived from the full-waveform inversion is M_W 3.5. In summary, the extensional character and the NE-SW orientation of the T-axis of the M_L 3.8 earthquake are consistent with other extensional mechanisms in the Penninic and Austroalpine domains of SE Switzerland (e.g., Kastrup et al. 2004; Marschall et al. 2013).

3.2.13 Salgesch (VS), 2016

The M_L 4.1 Salgesch earthquake was the strongest earthquake in 2015/16. It occurred about 6 km NE of Sierre on October 24th 2016 (14:44 UTC). The event was felt in large parts of Switzerland. Figure 10b indicates that the shaking intensity reached degree IV–V in the epicentral area, especially along the alluvium-filled Rhône valley. Intensity levels higher than III are apparent within about

Fig. 8 Seismicity within the Hegau-Bodensee graben in 2015/16. **a** Overview map with SED-routine hypocenter locations (blue circles: events in 2015; red circles: events in 2016) and mapped normal faults (after Egli et al. 2016). See box in Fig. 2 for location of the overview map. Nf: Neuhausen fault, Hg: Hegau graben; Rf: Randen fault; Sf: Schienerberg fault. **b** Map view of relative relocations of the Basadingen-Schlattingen (TG) sequence between September 2014 and May 2016 using double-difference techniques in combination with waveform cross-correlation. **c** Depth cross-section of the relocated Basadingen-Schlattingen sequence along a SW-NE striking profile AA'. Colors indicate origin time of the events. The focal mechanism of the M_L 2.2 event of May 31st is shown as lower hemisphere projection in map view and projected onto the depth profile in the cross-section. Relative relocations in combination with the focal mechanism suggest a NE dipping normal fault in the crystalline basement
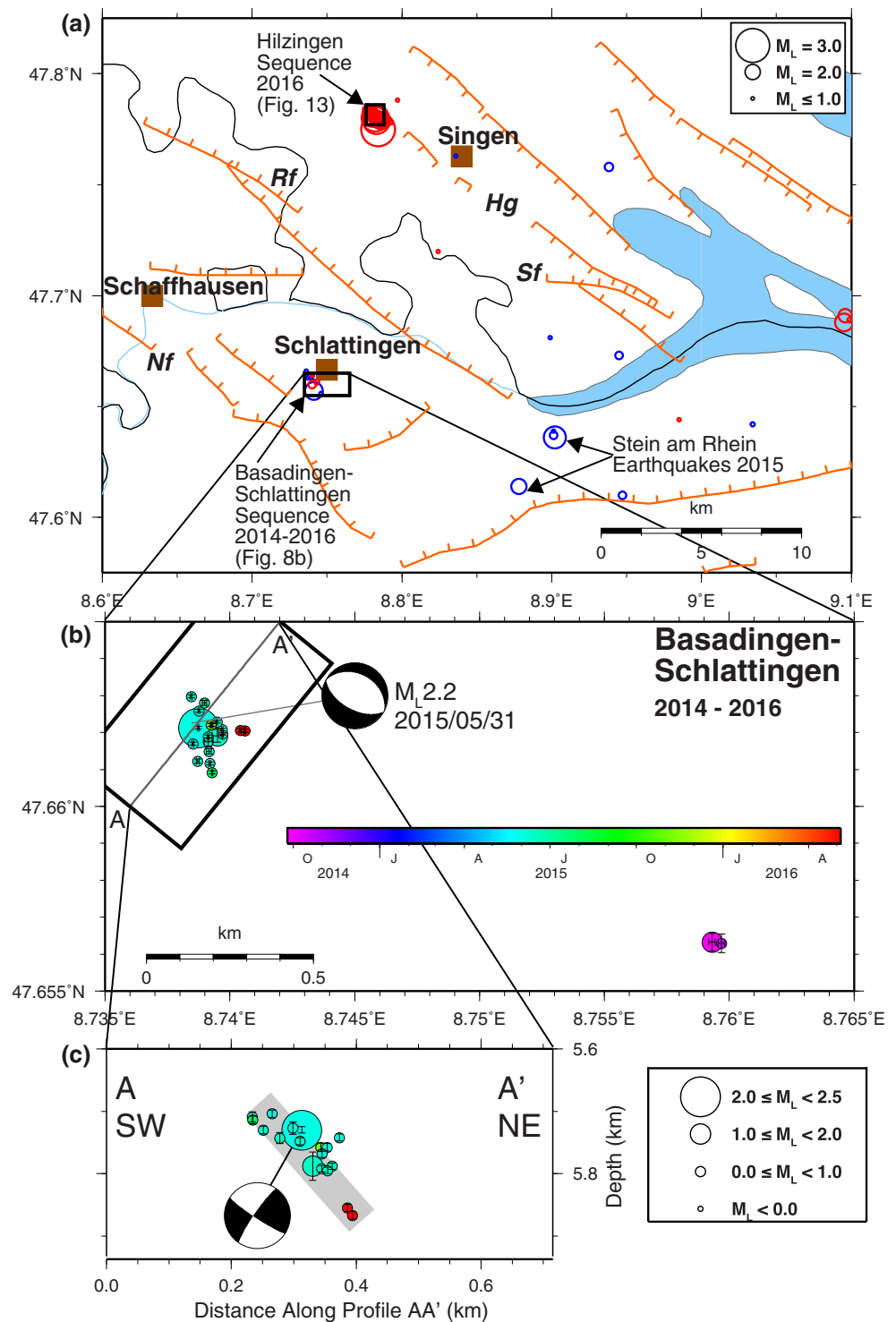
30 km of the epicentral location and along the lower Rhône valley. The comparison between the waveforms recorded in Sierre (strong-motion station SIEB) and Leukerbad (short-period station LKBD), both located at about 6 km epicentral distance, are amongst the most notable ground-motion observations for this event. Figure 11 shows the horizontal and vertical components of ground acceleration and velocity recorded at the two sites. All records were processed with acausal bandpass filters with a passband between 0.3 Hz and 80% of the Nyquist frequency (125 Hz at SIEB and 60 Hz at LKBD). As shown in Fig. 6c, station SIEB and LKBD locate in different parts of the focal sphere, with LKBD being close to nodal P and SIEB being close to nodal S, consistent with the S-to-P amplitude ratios
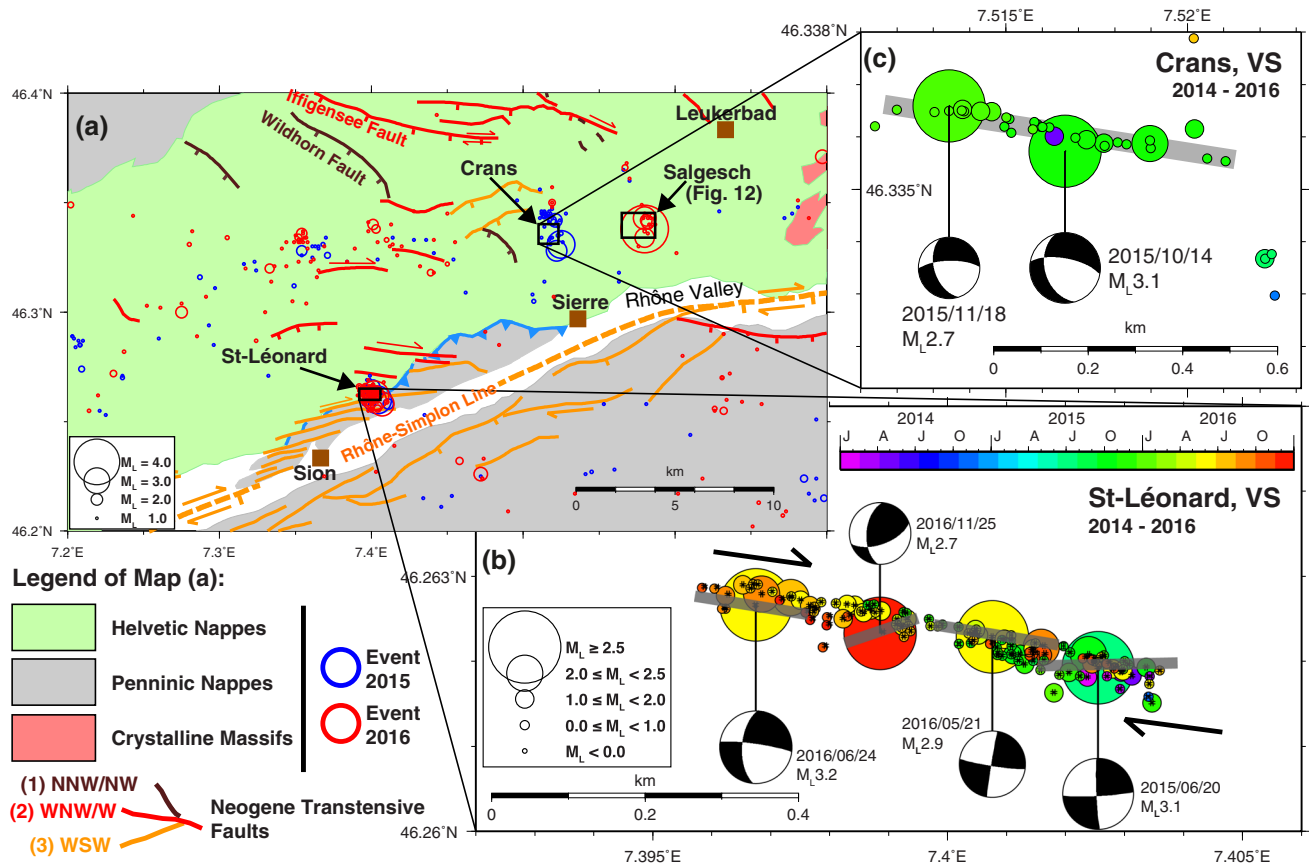
Fig. 9 Seismicity around the Rhône-Simplon Line between Sion and Sierre in 2015/16. **a** Overview map with SED-routine hypocenter locations (blue circles: events in 2015; red circles: events in 2016), main tectonic units and three sets of mapped transtensive faults (after Cardello and Mancktelow 2015). See box in Fig. 2 for location of the overview map. **b** Map view of relative relocations of the St-Léonard sequence in the period 2014–2016 using double-difference techniques. Crosses indicate relative location errors of epicenters. **c** Map view of relative relocations of the Crans sequence derived from double-difference techniques. Colors in **b** and **c** indicate origin time of the events. All focal mechanisms are shown as lower hemisphere projections

in Fig. 11. Station SIEB is located on colluvial deposits (SIA ground type B; $V_{S,30}$ about 725 m/s) at the edge of the Rhône alluvial plain. LKBD, on the other hand, lies on a limestone and schist rock cliff (Michel et al. 2014; stations.seismo.ethz.ch). Although the epicentral distance to both stations is similar, Fig. 11 documents significant differences in the acceleration waveforms, with peak ground acceleration values at SIEB being typically 10 times higher than those at LKBD. This exceptionally large amplification mainly concerns the high-frequency components of the ground-motion. The peak-ground velocity at SIEB is typically amplified by a factor of 2 only (on the horizontal components), consistent with the expected average amplification for this station given in the SED station database (stations.seismo.ethz.ch). Similar peak ground velocity yields similar macroseismic intensity levels in Fig. 10b. The aforementioned amplification of high frequencies is partly due to the local site response at SIEB. Additional source effects might also play a role, as SIEB is most likely

located on the hanging wall side of the causative fault (Fig. 9a).

The largest aftershock (M_L 2.8) occurred only 52 s after the mainshock (Table 1). In total, routine procedures detected only 16 aftershocks in October and November 2016. Magnitudes of aftershocks (excluding the immediate M_L 2.8 event) range between M_L 0.2 and 2.6. The focal depth of 8 km is well constrained by three stations located within 7 km from the epicenter. This focal depth suggests a source within the crystalline basement below the southern edge of the Helvetic nappes similar to the St. Léonard sequence. The fault plane solution derived for the M_L 4.1 Salgesch event, however, indicates a reverse fault mechanism with a small strike-slip component (Fig. 6c, Table S-4). The moment tensor solution is virtually identical with the first-motion solution (Fig. 6c). The moment magnitude derived from the full-waveform inversion is M_W 3.7. No focal mechanism could be calculated for the immediate M_L 2.8 aftershock, since P-phases were superimposed by the
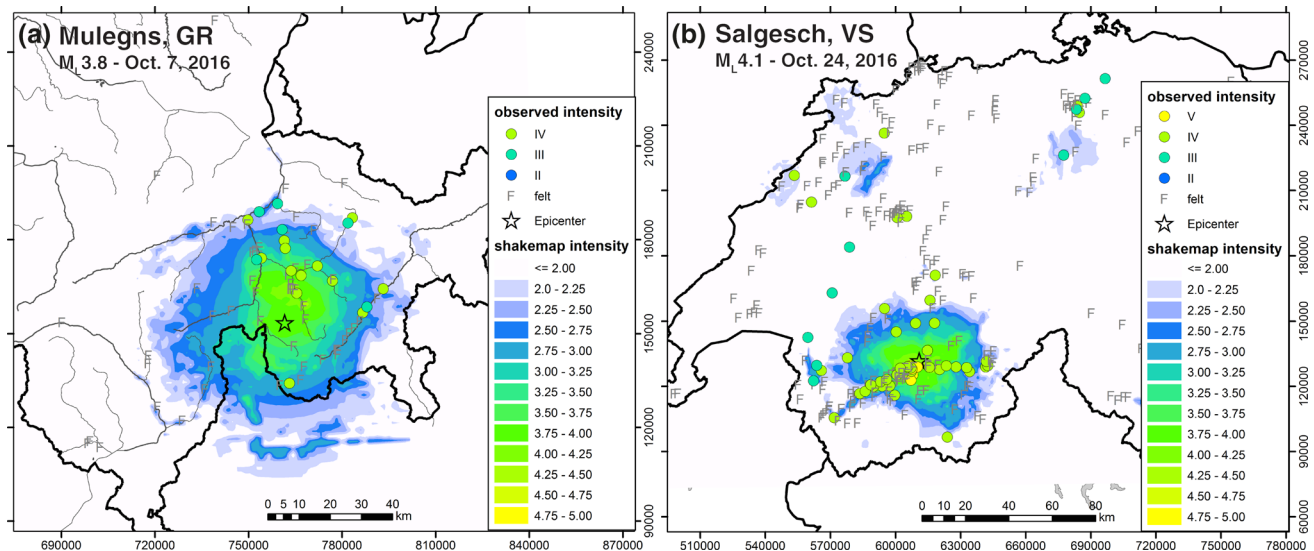
Fig. 10 ShakeMap with intensities converted from instrumentally recorded ground motions (background colors) and macroseismic intensities (EMS; Grünthal 1998) assessed by the SED based on felt reports submitted via the SED website (colored dots): **a** the M_L 3.8 Mulegns (GR) earthquake of October 7th 2016 (about 200 received felt reports in total); **b** the M_L 4.1 Salgesch (VS) earthquake of October 24th 2016 (about 780 received felt reports in total). The stars mark the earthquake epicenters

coda of the mainshock and the signal-to-noise ratio was too low to reliably determine first-motion polarities. A fault plane solution was obtained for the second largest aftershock (M_L 2.6) of October 25th 2016. The solution suggests an enlarged strike-slip component as well as differences in strike and dip compared to the mainshock (Fig. 6d). The focal mechanism of the mainshock is almost identical with the mechanisms of the M_L 3.9 Salgesch earthquake of April 5th 2003 (Deichmann et al. 2004), which suggests that both events are associated with the same fault. We performed a relative relocation of the earthquake cluster in order to image the active fault plane of the 2016 event and its relation to the 2003 rupture. We considered all earthquakes located in the area between 2002/01 and 2017/07. The resulting relocations are shown in Fig. 12. Profile AA', approximately oriented normal to the plane striking 65° (Fig. 6c), suggests that the active plane in 2016 was the SSE dipping plane (Fig. 12). The epicenter of the 2003 event locates about 300 m SW of the main cluster and projects within the cluster on the vertical profile (Fig. 12). Based on the similarity of the mechanisms and the spatial proximity in the relative locations we conclude that the 2003 and 2016 events are likely associated with the same fault.

3.2.14 Hilzingen (Germany), 2016

Between October 25th 2016 and January 20th 2017 a sequence of 60 (locatable) earthquakes occurred in Germany close to Singen, about 2 km north of the village of Hilzingen (Figs. 2b, 8a). The main episode of activity was

in November, with three events exceeding magnitudes of M_L 2.5 (Table 1). The strongest event of the sequence occurred on November 3rd and had a magnitude of M_L 3.0. It reached degree IV on the EMS scale and was felt within a radius of about 10 km distance (Stange et al. 2017). Focal depths of SED routine locations are 7 ± 1 km. The closest stations SCHS and STEIN (Fig. 1) are located in a distance of about 13 km from the epicentral region and focal depths are therefore less well constrained. In mid-November, the *Landeserdbebendienst Baden-Württemberg in Freiburg* (LED) installed a temporary station (HILZ) at about 2 km distance from the epicentral region in order to improve detection and location quality of the seismicity related to this sequence. The LED provided us with the data of the temporary station, and P and S-wave arrivals at station HILZ were picked for 24 events of the sequence. Focal depths of these 24 events systematically shifted to shallower depths of 4–5 km, consistent with the results of Stange et al. (2017), who report the sequence at a depth of about 5 km. The top of the crystalline basement is located at depths of about 2 km and less in the Hegau area (e.g., Egli et al. 2016). The focal depths of 4–5 km therefore suggest a source in the crystalline basement. A focal plane solution was derived for the M_L 2.7 event of November 19th (Fig. 5k, Table S-4), for which the depth (5 km) and the mechanism were constrained by additional data of the temporary station HILZ. To calculate consistent take-off angles for the less constrained M_L 3.0 event of November 3rd, we fixed its focal depth to 5 km, assuming that the event occurred on the same fault as the M_L 2.7 event. The derived solution (Fig. 5j) is similar to the one of the M_L 2.7

Fig. 11 Ground acceleration (top panels) and velocity (bottom panels) waveforms of the M_L 4.1 Salgesch (VS) earthquake of October 24th 2016 recorded at station SIEB (left column) and LKBD (right column) on different components. The processing of the waveforms is explained in the text
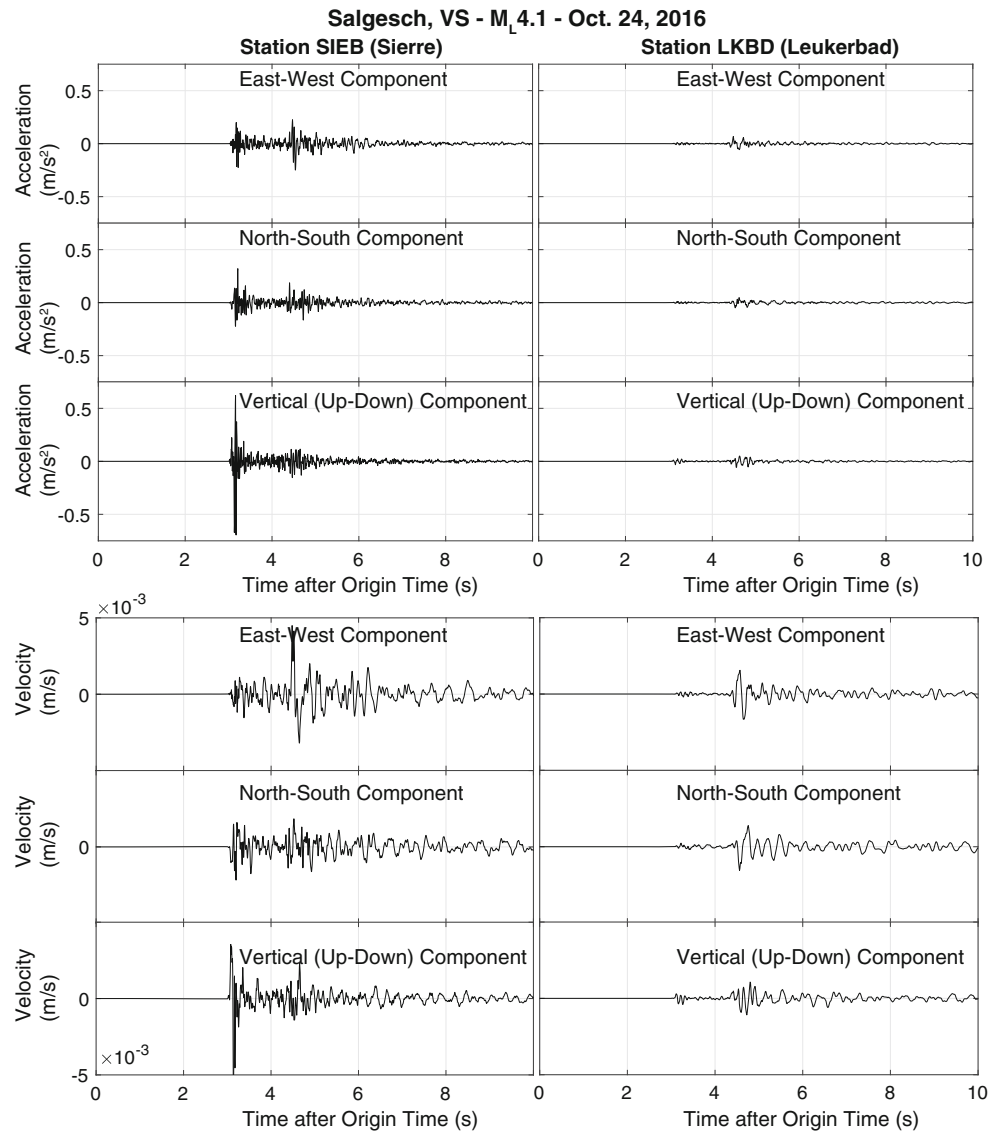

event, indicating a transtensional mechanism in both cases. Our results are also in good agreement with the fault plane solution of Stange et al. (2017), indicating a strike-slip mechanism with a normal component of similar orientation.

To constrain the active plane, we performed a relative relocation of the sequence. The results in Fig. 13 show that the seismicity forms a linear structure striking NW–SE, which determines the NW–SE striking dextral solutions in Fig. 5j, k as the active planes. Profile AA', oriented approximately normal to the strike of the dextral fault plane solutions (Fig. 13), clearly images a SW dipping fault, consistent with the focal mechanism. The relative locations along profile BB' suggest a vertical offset of 100–200 m between the M_L 3.0 event and the two M_L 2.7 events (Fig. 13), possibly indicating structural differences or stress heterogeneities along the fault. Seismicity migrates bilaterally along-strike from the center

towards SE and NW in the course of the sequence. The last events in January 2017 occurred at the NW tip of the structure.

The NW–SE striking Hilzingen sequence of 2016 locates about 2 km NE of an earthquake cluster, which was active in 1995 and 1996 ('Singen sequence', Deichmann et al. 2000). Based on relative relocations, this cluster was associated with a NNE dipping fault (Deichmann et al. 2000). Normal faults of similar NW–SE and WNW-ENE strike are mapped by geological and geophysical surveys and are associated with the Freiburg-Bonndorf-Bodensee Fault Zone (Fig. 8a) (e.g., Egli et al. 2016). The Hilzingen sequence of 2016 is probably related to a branch of the Hegau-Bodensee Graben, which vertically continuous into the crystalline basement (Fig. 8a). A detailed comparison of relocated seismicity with geologically and geophysically mapped structures of the Hegau-Bodensee Graben is planned in future.
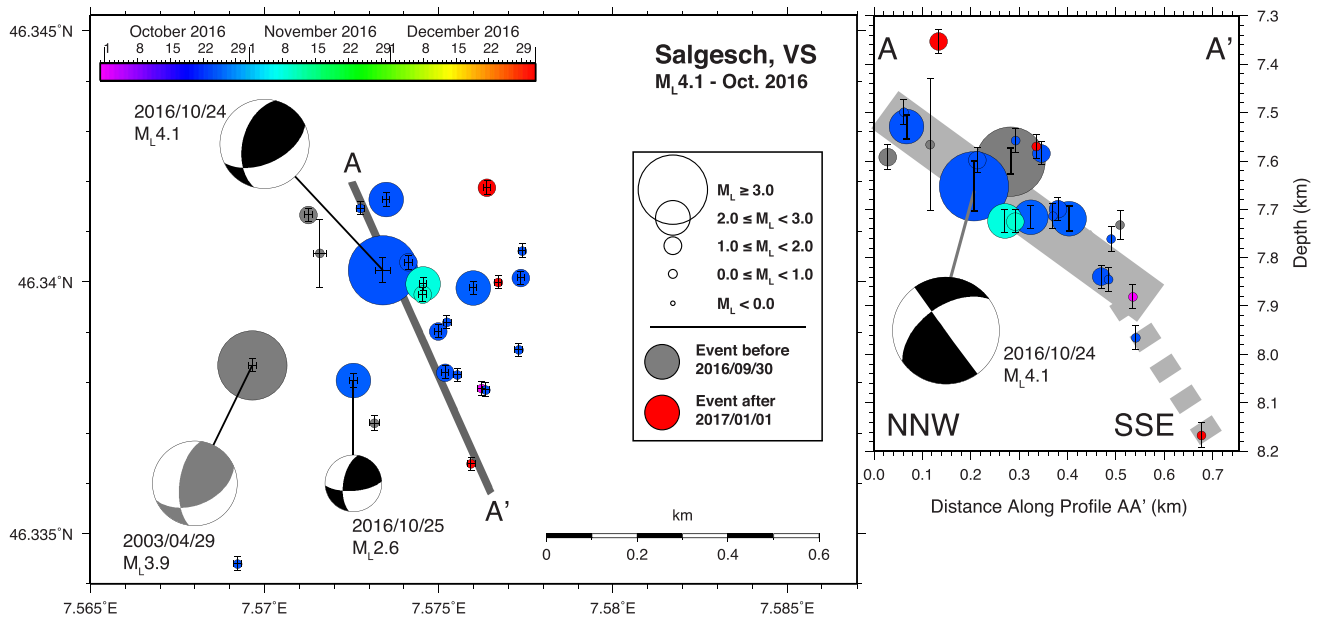
Fig. 12 Relative relocations of the Salgesch M_L 4.1 sequence and previous seismicity since 2002 using double-difference techniques in combination with waveform cross-correlation. Left: epicenters in map view and location of depth profile AA'; crosses indicate relative location errors of epicenters. Right: Depth profile AA'; vertical bars indicate relative location errors of focal depths. Focal mechanisms are shown as lower hemisphere projection in map view and projected to the depth profile in cross-section. Colors indicate origin time of the events

3.2.15 Novel (France), 2016

In December 2016, a series of $M_L \geq 2.5$ earthquakes occurred in the SE corner of Lake Geneva, close to the village of Novel (Fig. 2b). On December 22nd an M_L 3.0 as well as an M_L 3.4 earthquake occurred within 26 min (Table 1). Both events were felt in the region of Lake Geneva and in the Rhône valley to the east. Over the following 2 weeks, 13 additional earthquakes with magnitudes ranging between M_L 1.0 and M_L 2.9 were located in the same area. Routine hypocenter solutions as well as waveform characteristics indicate an unusually shallow source, likely within the sedimentary cover. The closest station is a temporary French AASN station (A173A) in about 8 km distance. Therefore the shallow depths are not reliably constrained. Consequently, the uncertainties in take-off angles are too large to unambiguously determine the focal mechanisms of these events.

3.3 Seismicity associated with the former deep heat mining project in Basel

Between 2010 and 2013, the seismic activity associated with the attempted stimulation of the Basel deep geothermal reservoir in 2006 occurred almost exclusively at the upper SSE periphery of the stimulated volume (Fig. S-3 in the Electronic Supplement; Diehl et al. 2014). Then, at the end of December 2014, the automatic monitoring system of the SED detected an M_L 1.6 event with a hypocenter located in a region that is closer to the casing shoe of the well, which had already been active in 2006 and 2007 (Fig. S-3; Diehl et al. 2015). At a magnitude level above the routine detection threshold, this region had been inactive since September 2007. Two additional smaller events with almost the exact same hypocenter location were detected using the template matching technique of Herrmann et al. (2017): one (M_L 0.6) occurred a few hours prior to the M_L 1.6 event of December 23rd, 2014, and the other (M_L 0.5) occurred on March 28th, 2015. A second cluster of three events (M_L 1.4, 1.2 and 0.7) occurred approximately in the same region between March 26th and May 24th, 2015 (Fig. S-3). Based on signal correlations, it is evident that two of these three events reactivated a small fault that had already been active on September 1st, 2007 with an M_L 1.5 event. In contrast to this renewed activity closer to the injection well, the other event recorded in 2015 (M_L 1.2) and the four events recorded in September and October 2016 (M_L between 0.9 and 1.9) were located—as in previous years—at the upper SSE periphery of the previously activated source volume. To lower the detection threshold, the template matching method of Herrmann et al. (2017) was applied to the continuous signals recorded by two of the
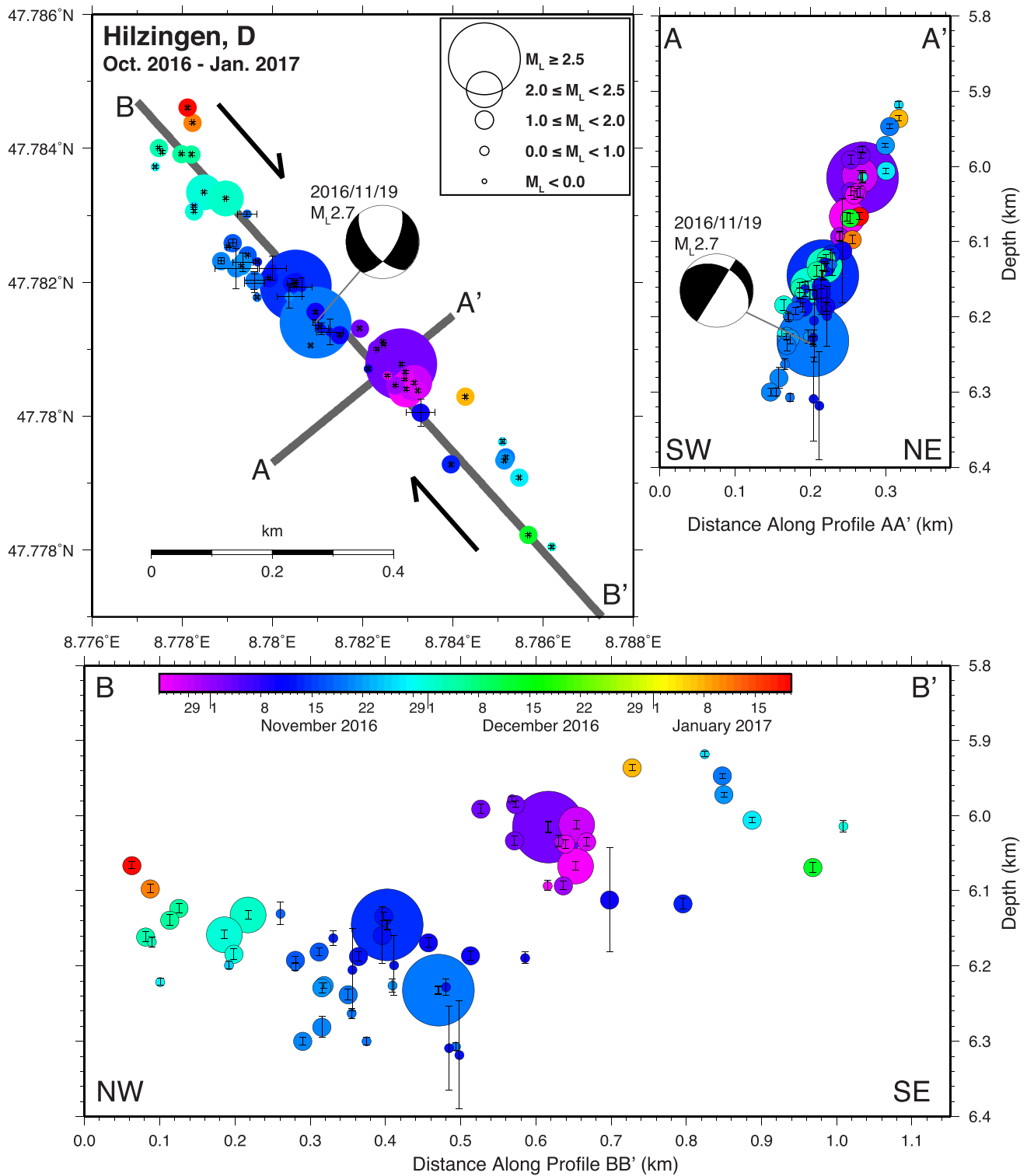
Fig. 13 Relative relocations of the Hilzingen sequence of 2016 using double-difference techniques in combination with waveform cross-correlation. Top Left: epicenters in map view and location of depth profiles AA' and BB'; crosses indicate relative location errors of epicenters. Top Right: Depth profile AA'; vertical bars indicate relative location errors of focal depths. Bottom: Along-strike profile BB'. Focal mechanisms are shown as lower hemisphere projection in map view and projected to the depth profile in cross-section. Colors indicate origin time of the events

borehole sensors still in operation (OTER2 and MATTE). Numerous smaller events that were detected by this method could be associated to the routinely recorded events at the periphery of the stimulated volume as well as in the newly reactivated region closer to the borehole (Herrmann et al. 2017). Thus this latter activity, which actually started already in 2013 with some weak precursors (Diehl et al. 2015), persisted in 2015 and 2016 and is evidence for a reactivation of a region closer to the borehole that was thought to have been relaxed following the stimulation in 2006. The additionally detected smaller events also show that the four routinely recorded events at the end of 2016 are only the high end of a general increase of the microseismic activity associated with the Basel geothermal well. The reasons for this increased activity were recently investigated in a comprehensive study and attributed to the gradual pressure increase in the borehole since it was sealed in April 2011 (Wiemer et al. 2017).

3.4 Rockfalls and rock avalanches in 2015/16

The SED detected two major rockfalls with its seismic network in 2016. On March 7th, a rockfall occurred at 17:52 UTC (18:52 local time) in the Val Calanca near Molina Buseno in Graubünden. The event with a reported volume of 5000 m^3 blocked the Val Calanca road across a length of approximately 200 m and its debris accumulated to a height of about 4 m. The seismic magnitude was estimated to be about M_L 1.0.

On September 11th, a rockfall occurred on the northern flank of Pizzo Cengalo at the head of Val Bondasca in southern Graubünden near the Italian border, with an equivalent seismic magnitude of M_L 2.1. The volume was estimated to be about 160,000–200,000 m^3. This unstable mountain flank was the location of a much larger rockfall in December 2011 (about 2 Mio. m^3, seismic magnitude M_L 2.7) and several minor events throughout the past years. The September 2016 event is the largest rockfall on this mountain since the 2011 collapse.

3.5 Notable non-earthquake seismic sources in 2015/16

On March 15th 2015, at around 20:46 CET (19:46 UTC), a bright meteor lit up the night sky, visible across southern Germany and northeastern Switzerland, and produced a sonic boom that was also widely noticed in Switzerland. The event was widely reported in the media. During the event, over a 4-min period, seismic sensors across the whole of northeastern Switzerland (in particular those located in shallow vaults) picked up signals from the sonic boom triggered by the falling meteorite on its trajectory from the North towards the Alps. A station near Andermatt, NALPS, first registered the sonic boom, suggesting any impact would have occurred in this region.

On August 29th 2016, a F/A-18 military jet of the Swiss Air Force crashed in the region of the Susten Pass (BE/UR) shortly after taking off from the Meiringen military airport. Stations within a radius of about 30 km recorded P and S waves, which are likely associated with the crash (Fig. S-4 in the Electronic Supplement). The travel-time inversion results in an impact location close to the reported site of crash and suggests that the impact occurred approximately at 14:03:37 UTC (16:03:37 local time).

4 Discussion and conclusion

In 2015/16, as in previous years, a large portion of the seismic activity was concentrated in the Valais, Graubünden, and their immediately adjacent regions (Fig. 2). As discussed in Diehl et al. (2015), the total number of located earthquakes per year has increased since 2013 due to ongoing densification of the seismic network, improvements in detection methods, and the occurrence of vigorous earthquake sequences. The same trend is observed for 2015 and 2016, for which the total number of events considerably exceeds the long-term average (Fig. 3). With a total of 20 earthquakes of magnitude $M_L \geq 2.5$, the seismic activity of potentially felt events in 2015 was slightly below the average of 23 earthquakes over the previous 40 years. With 31 events of magnitudes $M_L \geq 2.5$, we consider the seismic activity in 2016 to be above average.

The sequences of Basadingen-Schlattingen and Hilzingen provide new evidence for seismically active fault branches of the Hegau-Bodensee Graben, which likely root in the pre-Mesozoic basement. The 2014–2016 St-Léonard and the 2011 Sierre sequences suggest the existence of an en-echelon system of basement faults below the northern edge of the Rhône valley, which accommodates dextral slip along the Rhône-Simplon line in this area. Correlations in terms of strike and kinematics between the earthquake sequences of St. Léonard and Crans and faults mapped by Cardello and Mancktelow (2015) suggest a connection of seismogenic faults in the basement with outcropping faults at the surface of the Helvetic nappes. The transtensional mechanisms of events in the area of Crans-Montana on the one hand, and reverse to transpressional mechanisms observed for the M_L 4.1 Salgesch and M_L 2.7 St-Léonard earthquakes on the other hand, document the full complexity in structure and tectonic stresses north of the Rhône valley. The observed reverse and transpressional mechanisms might be expressions of restraining bends or step-

over zones of variable scales within a larger dextral fault array. Also stresses induced by vertical displacement, such as basement uplift, likely contribute to the complex strain regime in this region.

In 2016, two focal mechanisms provided new information on the internal deformation of the Aar massif. T-axes associated with the Jungfrau and Göschenen earthquakes suggest along-strike extension within the Aar massif, consistent with earlier evidence provided by the Lötschental earthquake of 1997 (Deichmann et al. 1998). Earthquakes like the M_L 3.8 Mulegns or the M_L 3.2 Bernina events in southeastern Switzerland and the adjacent region in Italy confirm the predominantly extensional neotectonic regime in the Penninic and Austroalpine domains in the eastern Swiss Alps (e.g., Marschall et al. 2013).

References

Aki, K., & Richards, P. G. (2002). *Quantitative seismology* (2nd ed., p. 704). South Orange: University Science Books.

AlpArray Seismic Network (2015): AlpArray Seismic Network (AASN) temporary component. *AlpArray Working Group.*

Other/Seismic Network. https://doi.org/10.12686/alparray/z3_2015.

Cara, M., Van der Woerd, J., Alasset, P.-J., Benjumea, J., & Mériaux, A.-S. (2017). The 1905 chamonix earthquakes: Active tectonics in the Mont Blanc and Aiguilles Rouges massifs. *Swiss Journal of Geosciences, 110,* 631–651. https://doi.org/10.1007/s00015-017-0262-7.

Cardello, G. L., & Mancktelow, N. S. (2015). Veining and post-nappe transtensional faulting in the SW Helvetic Alps (Switzerland). *Swiss Journal of Geosciences, 108,* 379–400. https://doi.org/10.1007/s00015-015-0199-7.

Cauzzi, C., Edwards, B., Fäh, D., Clinton, J., Wiemer, S., Kästli, P., et al. (2015). New predictive equations and site amplification estimates for the next-generation Swiss ShakeMaps. *Geophysical Journal International, 200,* 421–438. https://doi.org/10.1093/gji/ggu404.

Clinton, J., Cauzzi, C., Fäh, D., Michel, C., Zweifel, P., Olivieri, M., et al. (2011). The current state of strong motion monitoring in Switzerland. In S. Akkar, P. Gülkan, & T. van Eck (Eds.), *Earthquake data in engineering seismology: Predictive models, data management and networks (geotechnical, geological and earthquake engineering).* Dordrecht: Springer.

Deichmann, N., Baer, M., Ballarin Dolfin, D., Fäh, D., Flück, P., Kastrup, U., et al. (1998). Earthquakes in Switzerland and surrounding regions during 1997. *Eclogae Geologicae Helvetiae, 91*(2), 237–246.

Deichmann, N., Ballarin-Dolfin, D., & Kastrup, U. (2000). *Seismizität der Nord- und Zentralschweiz.* Wettingen: Nagra Technischer Bericht NTB 00-05.

Deichmann, N., Baer, M., Braunmiller, J., Cornou, C., Fäh, D., Giardini, D., et al. (2004). Earthquakes in Switzerland and surrounding regions during 2003. *Eclogae Geologicae Helvetiae: Swiss Journal of Geosciences, 97*(3), 447–458.

Deichmann, N., Baer, M., Braunmiller, J., Husen, S., Fäh, D., Giardini, D., et al. (2006). Earthquakes in Switzerland and surrounding regions during 2005. *Eclogae Geologicae Helvetiae: Swiss Journal of Geosciences, 99*(3), 443–452. https://doi.org/10.1007/s00015-006-1201-1.

Deichmann, N., Clinton, J., Husen, S., Edwards, B., Haslinger, F., Fäh, D., et al. (2012). Earthquakes in Switzerland and surrounding regions during 2011. *Swiss Journal of Geosciences, 105,* 463–476. https://doi.org/10.1007/s00015-012-0116-2.

Diehl, T., Deichmann, N., Clinton, J., Husen, S., Kraft, T., Plenkers, K., et al. (2013). Earthquakes in Switzerland and surrounding regions during 2012. *Swiss Journal of Geosciences, 106,* 543–558. https://doi.org/10.1007/s00015-013-0154-4.

Diehl, T., Clinton, J., Kraft, T., Husen, S., Plenkers, K., Guilhelm, A., et al. (2014). Earthquakes in Switzerland and surrounding regions during 2013. *Swiss Journal of Geosciences, 107,* 359–375. https://doi.org/10.1007/s00015-014-0171-y.

Diehl, T., Deichmann, N., Clinton, J., Kaestli, P., Cauzzi, C., Kraft, T., et al. (2015). Earthquakes in Switzerland and surrounding regions during 2014. *Swiss Journal of Geosciences, 108,* 425–443. https://doi.org/10.1007/s00015-015-0204-1.

Diehl, T., Kraft, T., Kissling, E., & Wiemer, S. (2017). The induced earthquake sequence related to the St. Gallen deep geothermal project (Switzerland): Fault reactivation and fluid interactions imaged by microseismicity. *Journal of Geophysical Research: Solid Earth, 122,* 7272–7290. https://doi.org/10.1002/2017JB014473.

Edwards, B., & Fäh, D. (2013). A stochastic ground-motion model for Switzerland. *Bulletin of the Seismological Society of America, 103,* 78–98. https://doi.org/10.1785/0120110331.

Edwards, B., Allmann, B., Fäh, D., & Clinton, J. (2010). Automatic computation of moment magnitudes for small earthquakes and the scaling of local to moment magnitude. *Geophysical Journal*

International, 183(1), 407–420. https://doi.org/10.1111/j.1365-246X.2010.04743.x.

Egli, D., Mosar, J., Ibele, T., & Madritsch, H. (2016). The role of precursory structures on tertiary deformation in the Black Forest—Hegau region. *International Journal of Earth Sciences, 106,* 2297–2318. https://doi.org/10.1007/s00531-016-1427-8.

Faenza, L., & Michelini, A. (2010). Regression analysis of MCS intensity and ground motion parameters in Italy and its application in ShakeMap. *Geophysical Journal International, 180,* 1138–1152. https://doi.org/10.1111/j.1365-246X.2009.04467.x.

Fäh, D., Giardini, D., Kästli, P., Deichmann, N., Gisler, M., Schwarz-Zanetti, G., Alvarez-Rubio, S., Sellami, S., Edwards, B., Allmann, B., Bethmann, F., Woessner, J., Gassner-Stamm, G., Fritsche, S., Eberhard, D. (2011). ECOS-09 earthquake catalogue of Switzerland release 2011 report and database, Public catalogue, 17.4.2011. Swiss Seismological Service ETH Zurich, Report SED/RISK/R/001/20110417.

Fäh, D., Moore, J. R., Burjanek, J., Iosifescu, I., Dalguer, L., Dupray, F., et al. (2012). Coupled seismogenic geohazards in Alpine regions. *Bollettino di Geofisica Teorica ed Applicata, 53*(4), 485–508. https://doi.org/10.4430/bgta0048.

Fréchet, J., Thouvenot, F., Frogneux, M., Deichmann, N., & Cara, M. (2010). The M_w 4.5 Vallorcine (French Alps) earthquake of 8 September 2005 and its complex aftershock sequence. *Journal of Seismology, 15,* 43–58. https://doi.org/10.1007/s10950-010-9205-8.

Grünthal, G. (1998). *European Macroseismic Scale 1998 (EMS-98)* (p. 99). Luxembourg: Cahiers du Centre Européen de Géodynamique et de Séismologie 15.

Hardebeck, J. L., & Shearer, P. M. (2002). A new method for determining first-motion focal mechanisms. *Bulletin of the Seismological Society of America, 92,* 2264–2276.

Herrmann, M., Kraft, T., Tormann, T., Scarabello, L. & Wiemer, S. (2017). A consistent high-resolution catalog of the induced earthquakes in Basel based on template matching. *2nd Schatzalp Workshop on Induced Seismicity*, 14-17 March 2017, Davos, Switzerland. http://www.seismo.ethz.ch/export/sites/sedsite/research-and-teaching/.galleries/pdf_schatzalp/P1-10_Herrmann.pdf.

Heuberger, S., Roth, P., Zingg, O., Naef, H., & Meier, B. P. (2016). The St. Gallen fault zone: A long-lived, multiphase structure in the North Alpine Foreland Basin revealed by 3D seismic data. *Swiss Journal of Geosciences, 109*(1), 83–102. https://doi.org/10.1007/s00015-016-0208-5.

Husen, S., and Hardebeck, J.L. (2010). Earthquake location accuracy, Community Online Resource for Statistical Seismicity Analysis. https://doi.org/10.5078/corssa-55815573. http://www.corssa.org.

Husen, S., Kissling, E., Deichmann, N., Wiemer, S., Giardini, D., & Baer, M. (2003). Probabilistic earthquake location in complex three-dimensional velocity models: application to Switzerland. *Journal of Geophysical Research, 108*(B2), 2077–2096.

Kastrup, U., Zoback, M.-L., Deichmann, N., Evans, K., Giardini, D., & Michael, A. J. (2004). Stress field variations in the Swiss Alps and the northern Alpine foreland derived from inversion of fault plane solutions. *Journal of Geophysical Research.* https://doi.org/10.1029/2003JB002550B01402.

Kraft, T., Mignan, A., & Giardini, D. (2013). Optimization of a large-scale microseismic monitoring network in northern Switzerland. *Geophysical Journal International, 195*(1), 474–490. https://doi.org/10.1093/gji/ggt225.

Lomax, A., Virieux, J., Volant, P., & Thierry-Berge, C. (2000). Probabilistic earthquake location in 3D and layered models. In C. H. Thurber & N. Rabinowitz (Eds.), *Advances in Seismic Event Location* (pp. 101–134). London: Kluwer Academic Publishers.

Madritsch, H. (2015). Outcrop-scale fracture systems in the Alpine foreland of central northern Switzerland: Kinematics and tectonic context. *Swiss Journal of Geosciences, 108,* 155–181. https://doi.org/10.1007/s00015-015-0203-2.

Marschall, I., Deichmann, N., & Marone, F. (2013). Earthquake focal mechanisms and stress orientations in the eastern Swiss Alps. *Swiss Journal of Geosciences, 106,* 79–90. https://doi.org/10.1007/s00015-013-0129-5.

Michel, C., Edwards, B., Poggi, V., Burjanek, J., Roten, D., Cauzzi, C., et al. (2014). Assessment of site effects in Alpine regions through systematic site characterization of seismic stations. *Bulletin of the Seismological Society of America, 104,* 2809–2826. https://doi.org/10.1785/0120140097.

Mock, S., & Herwegh, M. (2017). Tectonics of the central Swiss Molasse Basin: Post-Miocene transition to incipient thick-skinned tectonics? *Tectonics, 36,* 1699–1723. https://doi.org/10.1002/2017TC004584.

Molinari, I., Clinton, J., Kissling, E., Hetényi, G., Giardini, D., Stipčević, J., et al. (2016). Swiss-AlpArray temporary broadband seismic stations deployment and noise characterization. *Advances in Geosciences, 43,* 15–29. https://doi.org/10.5194/adgeo-43-15-2016.

Nagra, (2008). *Vorschlag geologischer Standortgebiete für das SMA- und das HAA-Lager-Geologische Grundlagen Textband.* Wettingen: Nagra Technischer Bericht NTB 08-04.

Nanjo, K. Z., Schorlemmer, D., Woessner, J., Wiemer, S., & Giardini, D. (2010). Earthquake detection capability of the Swiss Seismic Network. *Geophysical Journal International, 181,* 1713–1724. https://doi.org/10.1111/j.1365-246X.2010.04593.x.

Schorlemmer, D., & Woessner, J. (2008). Probability of detecting an earthquake. *Bulletin of the Seismological Society of America, 98*(5), 2103–2217. https://doi.org/10.1785/0120070105.

Stange, S., Hensch, M., Rodler, F.-A., Brüstle, W. (2017). Die Erdbebenserie im Hegau 2016/2017. Poster bei der 75. Jahrestagung der Deutschen Geophysikalischen Gesellschaft in Potsdam, 27–30.3.2017.

Swiss Seismological Service (SED) at ETH Zurich (1983): National Seismic Networks of Switzerland; *ETH Zürich.* Other/Seismic Network. https://doi.org/10.12686/sed/networks/ch.

Swisstopo, (2005). *Tektonische Karte der Schweiz 1:500000.* Wabern: Federal Office of Topography Swisstopo.

Vackář, J., Burjánek, J., Gallovič, F., Zahradník, J., & Clinton, J. (2017). Bayesian ISOLA: new tool for automated centroid moment tensor inversion. *Geophysical Journal International, 210,* 693–705. https://doi.org/10.1093/gji/ggx158.

Vouillamoz, N., Mosar, J., & Deichmann, N. (2017). Multi-scale imaging of a slow active fault zone: Contribution for improved seismic hazard assessment in the Swiss Alpine foreland. *Swiss Journal of Geoscience, 110,* 547. https://doi.org/10.1007/s00015-017-0269-0.

Waldhauser, F., & Ellsworth, W. L. (2000). A double-difference earthquake location algorithm: Method and application to the northern Hayward fault, California. *Bulletin of the Seismological Society of America, 90*(6), 1353–1368. https://doi.org/10.1785/0120000006.

Wehrens, P., Baumberger, R., Berger, A., & Herwegh, M. (2017). How is strain localized in a meta-granitoid, mid-crustal basement section? Spatial distribution of deformation in the central Aar massif (Switzerland). *Journal of Structural Geology, 94,* 47–67. https://doi.org/10.1016/j.jsg.2016.11.004.

Wiemer, S., Tormann, T., Herrmann, M., Karvounis, D., Kraft, T., & Marti, M. (2017) Induzierte Erdbeben im Nachgang des eingestellten Geothermieprojekts in Basel. Eine Analyse des Schweizerischen Erdbebendienstes (SED) an der ETH Zürich zu Händen des Kantons Basel-Stadt. http://www.seismo.ethz.ch/export/sites/sedsite/home/.galleries/pdf_home/Induzierte-

Erdbeben-im-Nachgang-des-eingestellen-Geothermieprojekts-in-Basel.pdf.

Worden, C. B, Wald, D. J. (2016). ShakeMap Manual. http://dx.doi.org/10.5066/F7D21VPQ.

Worden, C. B., Wald, D. J., Allen, T. I., Lin, K., Garcia, D., & Cua, G. (2010). A revised ground-motion and intensity interpolation scheme for ShakeMap. *Bulletin of the Seismological Society of America, 100,* 3083–3096. https://doi.org/10.1785/0120100101.